

Stellar-mass black holes in young massive and open stellar clusters and their role in gravitational-wave generation III: dissecting black hole dynamics

Sambaran Banerjee^{1,2}★

¹*Helmholtz-Institut für Strahlen- und Kernphysik (HISKP), Nussallee 14-16, D-53115 Bonn, Germany*

²*Argelander-Institut für Astronomie (AIfA), Auf dem Hügel 71, D-53121, Bonn, Germany*

September 21, 2018

ABSTRACT

Stellar-remnant black holes (BH) in dense stellar clusters comprise a natural setup to trigger general-relativistic (GR) inspiral and merger of binary black holes (BBH), detectable by the LISA and the LIGO-Virgo, through dynamical encounters inside such environments. In this work, the intricacies of such dynamical interactions are probed utilizing realistic, self-consistent, post-Newtonian, direct N-body evolutionary models of young massive and open stellar clusters. Particularly, the configurations of the compact subsystems, that drive the in-cluster GR BBH coalescences, are tracked on the fly. Such an approach reveals that the GR coalescences within the open clusters take place primarily via chaotic interactions involving triple BH systems. Although less frequently, such mergers are found to happen also in higher-order subsystems such as quadruples and in subsystems involving non-BH members; the mergers can themselves be BH–non-BH, which events would leave electromagnetic signatures. Close, fly-by encounters inside the clusters can also make BBHs and other types of double-compact binaries temporarily post-Newtonian; such binaries would potentially contribute to the GW background for the LISA and the PTA. These calculations, furthermore, suggest that open clusters are potential hosts for not only detached BH–main-sequence binaries, as recently identified in the globular cluster NGC 3201, but also a wide variety of other types of remnant–non-remnant binaries, which are assembled via dynamical interactions inside the clusters and which have the prospects of being discovered in radial-velocity surveys.

Key words: open clusters and associations: general – globular clusters: general – stars: kinematics and dynamics – stars: black holes – methods: numerical – gravitational waves

1 INTRODUCTION

Recent studies show that the retention of stellar-mass black holes (hereafter BH) in dense stellar clusters of wide mass range, beginning from low-/medium-mass young and open clusters (*e.g.*, Banerjee et al. 2010; Mapelli et al. 2011, 2013; Ziosi et al. 2014; Mapelli 2016; Park et al. 2017; Banerjee 2017; Mapelli et al. 2017; Banerjee 2018) through globular clusters (*e.g.*, Sippel & Hurley 2013; Morscher et al. 2013; Rodriguez et al. 2016; Chatterjee et al. 2017a; Wang et al. 2016; Askar et al. 2017) to galactic nuclear clusters (*e.g.*, Antonini & Rasio 2016; Arca-Sedda & Capuzzo-Dolcetta 2017; Hoang et al. 2018), make up environments where the BHs pair up through dynamical interactions which, furthermore,

potentially lead to general-relativistic (hereafter GR) coalescences of these binary black holes (hereafter BBH). Being much more massive compared to the rest of the stellar members in a cluster, the BHs sink and remain highly concentrated in the cluster’s central region (*e.g.*, Banerjee et al. 2010; Morscher et al. 2015) due to the dynamical friction (Spitzer 1987) from the stellar background, where they undergo frequent close and energetic encounters, giving rise to such events. That way, all the BBH merger events, as inferred so far through the detection of inspiral gravitational waves (hereafter GW) by the ground-based Advanced Laser Interferometer Gravitational-wave Observatory (hereafter LIGO) and the Virgo interferometric GW observatory (Abbott et al. 2016a,c,b; Abbott et al. 2017a,b,d), could be *naturally* reproduced (*e.g.*, Banerjee 2018, see also Mandel & Farmer 2017; Mapelli 2018). The “dynamical channel” would

★ E-mail: sambaran@astro.uni-bonn.de (SB)

easily sum up to a BBH merger detection rate of $\sim 100 \text{ yr}^{-1}$ by the LIGO at its proposed full sensitivity (see Banerjee 2017, 2018, and references therein).

Alternatively, BBH mergers, like those detected, can be derived through the evolution of isolated massive-stellar binaries in the field. Such a scenario typically involves a common-envelope (CE) phase, that tightens an initially-wide (semi-major-axis $a \sim 1000 \text{ AU}$) massive binary, combined with the formation of direct-collapse BHs (see Sec. 2.2) from the members (Belczynski et al. 2016; Stevenson et al. 2017; Belczynski et al. 2017). The alternative to this scenario involves chemically-homogeneous evolution of the members in a massive “over-contact” binary (MOB): here tidally-induced spins in the members of a close ($a \sim 100R_{\odot}$) massive binary allow them to become chemically mixed and helium rich throughout so as to avoid coalescence until they collapse into BHs (De Mink et al. 2009; De Mink & Mandel 2016; Marchant et al. 2016). In such studies, a low to a very high BBH inspiral detection rate of $\sim 10 - \sim 1000 \text{ yr}^{-1}$ has been estimated for the full-sensitivity LIGO.

Recent studies by Banerjee (2017, hereafter Paper I) and Banerjee (2018, hereafter Paper II) have shown, for the first time through detailed and completely self-consistent relativistic (post-Newtonian; hereafter PN) direct N-body simulations, the importance of triple-/higher-order-dynamical interactions in triggering in-cluster GR BBH coalescences, particularly inside low-velocity-dispersion systems such as open clusters and lower-mass globular clusters (hereafter GC)¹. A lower velocity dispersion makes gravitational focusing (Spitzer 1987) generally more efficient, especially when the most massive cluster members such as the BHs are involved, facilitating the dynamical formation of triple and higher-order multiple systems comprising (but not limited to) them. Such dynamically-formed subsystems are also generally wider in a lower velocity-dispersion environment, due to the lower hard-soft energy boundary (Spitzer 1987), making the subsystems’ geometrical cross sections larger. The efficient gravitational focussing and larger geometric cross section make the subsystems both highly efficient in undergoing dynamical interactions, potentially competing in frequency with those involving only singles and binaries (Leigh & Geller 2013), and highly vulnerable to close, dynamical encounters leading to their significant alteration or destruction (“dynamical interruption”; Geller & Leigh 2015). Hence, the success of a GR coalescence within a triple or a higher-order multiple system often relies on the large eccentricity growth in chaotic encounters, during either a resonant binary-single interaction (Hut & Bahcall 1983; Samsing et al. 2014) or a chaotic phase of the evolution of a hierarchical triple (higher-order multiple; e.g., Antonini et al. 2016), rather than the secular evolution of a compact subsystem, e.g., the (eccentric) Kozai-Lidov (hereafter KL) oscillation of a triple (Kozai 1962; Katz et al. 2011; Lithwick & Naoz 2011). The timescales of eccentricity boost during the chaotic processes are, typically, much shorter compared to the secular timescales of the compact subsystem, fostering the opportunity for rapid GR inspiral and merger before the

subsystem can be significantly altered or destroyed by the next close encounter. Note that such triples can form as a result of both binary-single and binary-binary geometrically-overlapping or close encounters (see, e.g., Heggie & Hut 2003; Sigurdsson & Phinney 1993; Leigh & Sills 2011). As estimated in Paper II based on conservative assumptions, the possibility of triple-mediated, in-cluster BBH coalescences combined with their abundance would make the contribution of open clusters, to the dynamical BBH merger rate, comparable to those from the GCs and nuclear clusters.

In fact, a substantial increase in such in-cluster BBH mergers has been demonstrated even for GC-like systems in subsequent semi-analytic and Monte Carlo studies when PN effects are incorporated (Samsing 2018; Rodriguez et al. 2018). Given that any BBH (as such, any binary) that remains bound to the cluster for a while is necessarily hard (Heggie & Hut 2003), close, *fly-by* binary-single encounters would typically *not* cause sufficient eccentricity growth of the BBH so that it can promptly undergo GR inspiral and merger before the next close encounter; however, the dynamically-induced eccentricity can still be sufficient to make the BBH “temporarily relativistic” (see Secs. 2.3 & 3.2). Of course, if a BBH (or even a BH-neutron star; hereafter NS or NS-NS binary) ends up getting ejected from the host cluster as the outcome of a resonant or a fly-by binary-single interaction or a chaotic breakup of a triple, then, given sufficient tightness and eccentricity, it will have time until the current epoch for merging (Banerjee et al. 2010; Askar et al. 2017; Rodriguez et al. 2016; Chatterjee et al. 2017b). Massive GCs, with velocity dispersion typically $\sim 10 \text{ km s}^{-1}$ and moderate escape velocities, which host fairly tight BBHs that are also sufficiently dynamically active, are the most efficient machines for ejecting such “merge-able” BBHs.

Such intricacies of the dynamical interactions in stellar clusters that lead to BBH and possibly also other types of GR binary coalescences make it tempting to follow them *live* (i.e., on the fly) in evolutionary cluster models comprising realistic ingredients in a fully self-consistent manner, which motivates the current Paper III. Perhaps more importantly, such a study, which is for the first time of its kind, will be directly useful for interpreting the existing and the forthcoming inspiral GW detections by the LIGO-Virgo and as well the GW signals from BBHs detected by the forthcoming space-based interferometric GW observatory Laser Interferometer Space Antenna (hereafter LISA Amaro-Seoane et al. 2017). It will as well aid the anticipations and the interpretations of combined LISA-LIGO BBH inspiral detections and BBH eccentricity detections in the LISA band (Sesana 2016; Nishizawa et al. 2017; Banerjee 2018). In particular, for the first time from ab initio, long-term, relativistic, direct N-body simulations, Banerjee (2018, see their Fig. 7) has shown that all on-the-fly-detected, in-cluster BBH in-spirals and at least half of the ejected BBH in-spirals pass through high eccentricities ($e > 0.1$), but not too high to be inaudible ($e \lesssim 0.7$; Chen & Amaro-Seoane 2017), in the LISA’s characteristic detection band. Similar conclusions have subsequently been arrived at in Monte Carlo and semi-analytical studies such as Kremer et al. (2018a); Samsing & D’Orazio (2018). Note that until now the configuration and evolution of relativistic triple systems have been probed in the field (e.g. Silsbee & Tremaine 2017; Antonini et al. 2017), “isolated” from their parent globular or open clusters to study

¹ See also the related blog article from the Oxford University Press: <https://blog.oup.com/2017/03/dance-of-black-holes/>.

them separately (*e.g.* Kimpson et al. 2016; Antonini et al. 2016), or such triples have been formed in three-body scattering experiments (*e.g.*, Samsing et al. 2014; Samsing & Ramirez-Ruiz 2017). From a pedagogical point of view, a live investigation of relativistic subsystems, that continue to form and destroy in a dynamically-active environment such as inside a dense star cluster, will lead to a better understanding of the dynamical interactions that cause extreme GR effects in an otherwise Newtonian system.

The current study, which is a preliminary step towards such “hands-on” probe into the internal mechanics of BH subsystems in stellar clusters, involves *ab initio*, long-term, relativistic, direct N-body computations of young massive and open clusters along the lines of Paper II (Sec. 2). The enhancement and diversity of dynamical interactions and their consequences, due to the inclusion of even a small fraction of primordial binaries, has been conceived in Paper II: in this work, a wider range of primordial-binary fraction is considered (5%-50%; Sec. 2). Also, a wide initial-mass range of the primordial binary-containing models are considered ($7.5 \times 10^3 M_{\odot} - 5.0 \times 10^4 M_{\odot}$; Sec. 2).

Furthermore, in some of the runs here, specialized output arrangements are made to record the configuration of the triple/higher-order-multiple system hosting a GR coalescence (Sec. 2.3.1): this is one step forward towards on-the-fly probing of GR-merger-hosting subsystems (Sec. 3.1) and also GR—fly-by interactions (Sec. 3.2) within the clusters. Also, the “ambient” population of BBHs, as a function of the host cluster’s properties, is investigated here in detail (Sec. 3.3).

Apart from the BBHs and their mergers, the formation of BH–non-BH binaries, and, in particular, of detached BH–main sequence (hereafter MS) binaries are looked at in this work. The recent discovery of a detached ($a \gtrsim 1$ AU) BH–MS binary in the GC NGC 3201 by Giesers et al. (2018), through radial-velocity measurements, has generated high interest in theoretically investigating formation channels of such binaries in GCs (Askar et al. 2018; Kremer et al. 2018c). Other GCs, where stellar-mass BH candidates accreting from stellar companions have been identified through radio and X-ray observations, are M22 (Strader et al. 2012), M62 (Chomiuk et al. 2013), 47 Tuc (Miller-Jones et al. 2015), and M10 (Shishkovsky et al. 2018); the potential donor companion has also been optically identified for the M10 object which is a “red straggler” star. It is natural to expect that the dynamically-active environment of young massive and open clusters would as well give rise to such binaries, which is also investigated in this work (Sec. 3.4). The results are recapitulated in Sec. 4.

2 MODEL COMPUTATIONS

Table 1 summarizes the model computations: some of the computations from Paper II are recycled here, which are indicated in Table 1. The computed models *initiate* with Plummer (1911) profiles with masses $7.5 \times 10^3 M_{\odot} \lesssim M_{cl}(0) \lesssim 5.0 \times 10^4 M_{\odot}$, half-mass radii $1.0 \text{ pc} \lesssim r_h(0) \lesssim 2.0 \text{ pc}$, *overall* (see Sec. 2.1) primordial-binary fractions (the fraction of the total number of stars in binaries initially) $0.05 \lesssim f_{\text{bin}}(0) \lesssim 0.5$, and have metallicities $0.001 \leq Z \leq 0.02$. All the computed models are taken to be initially unsegregated and are sub-

jected to a solar-neighbourhood-like external galactic field. In this work, some stress is provided to the models in the lower side of the covered mass range, which initiate with a high fraction of primordial binaries ($f_{\text{bin}}(0) \gtrsim 0.3$; see Sec. 2.1, Table 1). Since these models are time consuming (and challenging) to run for long term, only $Z = 0.02$ and 0.001 are considered for them; the BH mass distribution, that is retained in the cluster at birth (see Sec. 2.2), does not depend strongly on Z at its sub-solar values (see, *e.g.*, Fig. 1 of Banerjee 2017) so that a $Z = 0.001$ model would serve to mimic typical $Z < Z_{\odot}$ clusters, *e.g.*, as in dwarf galaxies.

Such model clusters represent young massive and open clusters that continue to form and dissolve throughout a gas-rich galaxy, as in, *e.g.*, the Milky Way and the other Local Group galaxies. Therefore, considering only a solar-neighbourhood-like external field ignores the fact that such a cluster may be subjected to a much stronger galactic field that would accelerate its dissolution. However, recent test computations (Riaz et al., in preparation) suggest that such clusters continue to produce relativistic subsystems and mergers (see Secs. 3.1 & 3.2) even when they orbit at 1 kpc Galactocentric radius as long as they survive long enough to allow the BHs in them to become centrally segregated and hence dynamically active (Banerjee et al. 2010). A larger set of models covering a range of external field will be undertaken in a future study.

2.1 Introduction of primordial binaries

Although having $f_{\text{bin}}(0)$ as high as 0.5 makes the long-term direct N-body computations, as done here (see below), quite challenging, it has the potential to generate BBH coalescences even in the least massive models, due to the enhanced BBH formation through exchange encounters (see Paper II). More importantly, as observations imply, intermediate- and old-aged open clusters typically have significantly higher primordial-binary fractions than those in GCs (Leigh et al. 2015) — often several 10s of percent (Khalaj & Baumgardt 2013; Milliman et al. 2014; Geller et al. 2015). Hence, assuming such high $f_{\text{bin}}(0)$ is as well more realistic. For computational ease, only the $M_{cl}(0) \approx 7.5 \times 10^3 M_{\odot}$ and $1.5 \times 10^4 M_{\odot}$ models are computed with $f_{\text{bin}}(0) > 0.1$, in this study.

Note that the values of $f_{\text{bin}}(0)$ as quoted above and in Table 1 represent the *overall* initial binary fraction in the cluster for the entire stellar mass distribution, the latter being taken to be canonical (Kroupa 2001). However, as in Paper II (see their Sec. 2), the initial binary fraction of the O-type stars (stellar mass, $m_s \gtrsim 16 M_{\odot}$), taken separately, is $f_{\text{Obin}}(0) \approx 100\%$, to be consistent with the observed high binary fraction among O-type stars in young clusters and associations (see, *e.g.*, Sana & Evans 2011; Sana et al. 2013). As elaborated there, the O-type-stellar binaries are taken to initially obey the orbital-period distribution of Sana & Evans (2011) and a uniform mass-ratio distribution (an O-star is paired only with another O-star, as typically observed, and the pairing among the lower-mass stars is obtained separately; see below). The orbital periods of the non-O-star primordial binaries are taken to follow a Duquennoy & Mayor (1991) distribution that represents a dynamically-processed binary population (Kroupa 1995), and their mass-ratio distribution is also taken to be uniform. The initial binary fraction among the non-O-type stars is taken to be $f_{\text{bin}}(0)$; since

for the adopted canonical IMF the non-O-type stars comprise by far the majority of the stellar population, the overall initial binary fraction is also $\approx f_{\text{bin}}(0)$. As in Paper II, the initial eccentricities of the O-type stellar binaries follow the Sana & Evans (2011) eccentricity distribution and those for the rest of the binaries are drawn from the thermal eccentricity distribution (Spitzer 1987). As explained in Paper II, such a scheme of including primordial binaries provides a reasonable compromise between the economy of computing and consistencies with observations.

2.2 Stellar remnant formation

In this work, stellar-remnant NSs and BHs are formed as in Papers I & II, *i.e.*, with a modified version of the semi-analytical binary-stellar-evolutionary program BSE (Hurley et al. 2000, 2002) which is coupled to the N-body program (see Sec. 2.3) that evolves the stars and stellar binaries from their zero age until remnant formation in tandem with the dynamical evolution; see Sec. 2.2 of Paper I and references therein for a detailed description. Here, direct-collapse BHs (hereafter DCBH) and electron-capture-supernova (hereafter ECS; Podsiadlowski et al. 2004) NSs, whose natal kicks are taken to be zero, retain in the clusters at birth and participate in dynamical interactions for long term. In the presence of massive primordial binaries, as in here, the mass distribution of the BHs are moderately influenced by massive-binary coalescences, the occurrences of which can be dynamically-influenced (see Sec. 2.1 of Paper II). As elaborated in Paper I (see their Sec. 2.2), the DCBHs are formed based on the supernova-fallback results of Fryer (1999); Fryer & Kalogera (2001) which, as well as the formation of ECS-NSs, are implemented in BSE in similar ways as in Belczynski et al. (2008, 2010).

Note that the evolution of a binary containing at least one non-compact star, be it detached or Roche-lobe overflow (hereafter RLO), is affected both by stellar-evolutionary mass loss and dynamical encounters; also by mass transfer, for the RLO binaries. However, in the majority of the model computations in Table 1, the optional tidal interactions among single stars and within a binary, as implemented in NBODY7 according to the prescriptions described in Mardling & Aarseth (2001), is disabled. Such tidal energy dissipation schemes, in addition to being generally poorly understood, apply only to low-mass stars. The tidal interaction would mainly affect a handful of very tight primordially-derived binaries (orbital period $\lesssim 10$ days) that anyway project negligible cross sections for dynamical interactions and would typically not play a role for the formation and/or modification of the much wider dynamically-formed/dynamically-active binaries. However, the members of such a dynamically-formed/dynamically-active binary can also interact tidally at the periastron provided the binary is sufficiently eccentric; that way, it can circularize and undergo orbital decay even up to the point of RLO (Kremer et al. 2018b). Therefore, to see whether tidal dissipation would influence the dynamical formation and the properties of BH-MS binaries, a set of test, shorter-term runs are performed for three of the $Z = 0.02$ initial models with tidal dissipation activated, as indicated in Table 1. Tidal dissipation may also likewise tighten a fraction of the star-star

binaries, resulting in tighter BBH and BH-NSs through exchange encounters².

Note that according to the adopted primordial-binary population (Sec. 2.1), all of the BH progenitor stars are initially in massive binaries. However, the members' mass loss until BH formation widens the binaries significantly, which are then dissociated in a dynamically-active environment (Morscher et al. 2015; Chatterjee et al. 2017a), resulting in predominantly single BHs. Furthermore, strong dynamical encounters would often impart high eccentricities onto a massive binary (see Sec. 1), potentially resulting its members' merger into a single star; if the merger happens after the members have already evolved until close to the remnant formation, the single BH resulting from the merger product can be substantially more massive than what a dynamically-inert population of single stars with the same zero-age mass range would yield (see Fig. 1 or Paper II). Nevertheless, a few of the massive primordial pairs may survive even after both members have become BHs - the properties of such primordially-derived BBHs are discussed in Sec. 3.3. Apart from these, any BBH existing inside a cluster must have been dynamically paired, as discussed in Sec. 3.3.

Finally, note that although in the present study the BH population within a cluster, that participates in dynamical encounters, is derived via a specific recipe (see above) the qualitative aspects of the outcomes, especially those of the GR mergers and close encounters (Secs. 3.1 & 3.2), are likely to hold true if the BHs' natal mass distribution is altered; in particular, if it is widened. This is because the present BH mass distribution is already wide by several factors, especially at low metallicities (see Figs. 1 of Papers I & II). However, if one or two of the retaining BHs are distinctly more massive than the rest, say, be intermediate-mass black holes (IMBH; *e.g.* Lützgendorf et al. 2016), then the BH triples/multiples can be additionally dissociated by the IMBH(s) (Leigh et al. 2014), and (intermediate-mass-ratio) inspirals (IMRI) onto them may be favoured. A detailed study of the latter case is beyond the scope of this paper.

2.3 The post-Newtonian, direct N-body evolution program NBODY7 : live tracking of relativistic interactions and subsystems

As in Paper I & II, the state-of-the-art, relativistic, direct N-body evolution program NBODY7 (Aarseth 2003; Nitadori & Aarseth 2012; Aarseth 2012) is utilized to evolve these initial models. The key aspects of the code are summarized in Sec. 2.1 of Paper II. In brief, NBODY7 is a fourth-order Hermite integrator for member-by-member tracking of trajectories in an arbitrary, self-gravitating, many-body system where the close encounters and the bound subsystems (binaries and multiples) are treated with *regularization tech-*

² In NBODY7, `option 27 = 1/2` and `3` applies tidal dissipation and GW-radiation dissipation mutually exclusively on a KS-regularized pair (Sec. 2.3). However, since in the present runs, the compact subsystems as well as the PN binaries are always treated with the ARC (`option 11 = -1` used; Sec. 2.3), no compromise is made with the PN treatment of a binary or a higher-order subsystem even if the tidal-dissipation `option` is chosen for the KS pairs (`option 27 = 1`).

niques and no force softening is applied. The integration is facilitated by applying a neighbour-based scheme (Nitadori & Aarseth 2012) for the force contributions at the shortest time intervals (the “irregular” force/steps). At longer intervals (the “regular” force/steps), all bound members in the system are included for the force evaluation. The irregular forces are computed by parallel processing in CPUs, while the much more expensive regular forces are evaluated on GPUs³. The near-diverging gravitational forces during two-body close passages and in binaries are dealt with two-body or Kustaanheimo-Stiefel (KS) regularization (Aarseth 2003) and higher-membership interactions/multiples are treated with the Algorithmic Regularization Chain (ARC; Mikkola & Tanikawa 1999; Mikkola & Aarseth 2002; Mikkola & Merritt 2008). As opposed to the traditional or KS-Chain Regularization (Mikkola & Aarseth 1993), the adoption of the ARC in NBODY7 allows the inclusion of members in arbitrary mass ratios, in the Chain. This is particularly necessary for the present calculations where the BHs span a wide mass range and predominantly take part in binary-single and binary-binary interactions (see Sec. 1, Papers I & II).

In NBODY7, the Chain members and the Chain perturbers are, nevertheless, selected in the same well-proven way as in the standard KS-Chain implementation (Aarseth 2003, 2012), except that the internal integration of the Chain is done in the ARC way (Mikkola & Merritt 2008 and references therein). Here, the Chain members, that comprise a compact subsystem (often a triple or a quadruple), are initially chosen based on the strategies for identifying hierarchical systems. This comprises identifying, for each member in the system, the dominant and the next-to-dominant perturber and testing whether to form a triple or a quadruple; see Chapter 9 and Algorithm 11.3 of Aarseth (2003) for the details. The Chain is then constructed (and possibly switched during the Chain integration due to either change in the subsystem’s configuration or the close approach of a perturber) in the usual way by sequentially connecting the closest subsystem members with vectors as described in Mikkola & Aarseth (1993). The perturbers of the Chain are then selected either from within its close-encounter radius or through a full perturber search. The key algorithms are discussed in Chapter 12 of Aarseth (2003).

An important aspect of NBODY7 is its GR treatment of binaries and multiples (and also of close two-body encounters) involving a BH or an NS through the ARC (Mikkola & Merritt 2008). This enables on-the-fly GR orbital modifications and coalescences of relativistic subsystems (typically, but not limited to, a binary or a triple containing one or more BH/NS) that are bound to the system. In principle, PN-1, PN-2 (GR periastron precession), PN-2.5 (orbital shrinking due to GW radiation), PN-3, and PN-3.5 order terms can be included in the ARC procedure, including their spin contributions. However, for computational ease, the BHs’ spins are taken to be zero in the present computations. The spin terms would have moderately affected the times of the GR coalescences occurring within the cluster (see Sec. 1), how-

ever, this is not critical here due to the statistical nature of the dynamically-induced BBH coalescences.

Furthermore, in practice when the stellar-remnant BHs have large spins, a BBH would typically receive a large GW merger kick during its final inspiral and plunge ($\sim 100 - 1000 \text{ km s}^{-1}$; Campanelli et al. 2007; Hughes 2009). This would cause almost all the newly-formed, merged BHs to escape from open and globular clusters almost immediately, without having a chance to participate in dynamical encounters further. This effect is mimicked in NBODY7 by applying a velocity kick onto the merged BH immediately after a GR BBH coalescence occurs within the cluster (Sec. 3.1). In the current implementation, the applied kick is kept only marginally above the escape speed to avoid large energy errors, ≈ 5 times the central RMS speed, which is enough to eject the merged BH out of the cluster; in reality a BBH merger product would typically escape at a much higher speed⁴.

To accommodate the possibility of a pure KS compact binary becoming relativistic, say, due to a strong fly-by encounter that imparts a high eccentricity onto it (see also Samsing et al. 2014 in this context), GR orbital modifications are included in the KS treatment as well. Such encounters, which are termed here as “GR slingshot”s, do take place in the model computations presented here, although relatively rarely (see Sec. 3.2). However, in these NBODY7 calculations, the two-body GR systems are also treated via the ARC (option 11 = -1 used). As pointed out in Sec. 1, GR slingshots would mostly give rise to temporarily-relativistic binaries but are unlikely to lead to GR coalescences, as found in the model computations presented in Table 1.

As in Papers I & II, the physical speed of light has been used in all the newer computations in this work, except for one particular test computation with $M_{cl}(0) \approx 1.5 \times 10^4 M_{\odot}$, $r_h(0) \approx 1.5 \text{ pc}$, $Z = 0.001$, and $f_{bin}(0) \approx 0.05$, where $c/100$ is assumed (see Table 1).

2.3.1 Extracting (relativistic) Chain compact subsystems in NBODY7

As discussed in Sec. 1, it would be interesting and useful to probe the compact subsystems in which the GR BBH and, possibly, other types of compact-binary mergers occur. More generally, it would be useful to extract the spectrum of GR subsystems that continue to appear (and disappear) within a model cluster over its evolution; they would collectively contribute to the total GW output from the cluster and a subset of them may potentially serve as semi-persistent sources for the LISA and the Pulsar Timing Array (hereafter PTA; Hobbs et al. 2010). Furthermore, at least for the Galactic and Local Group clusters, the population of relativistic subsystems in them may, potentially, contribute to

³ All simulations in this work are done on server-class workstations equipped with quad-core AMD processors and NVIDIA’s Fermi and Kepler series GPUs.

⁴ Alternatively, the LIGO-observed BBH mergers to date may suggest zero or small spins of the BHs participating in the mergers (Farr et al. 2017). In that case, the merger product would likely be retained in open clusters and GCs, potentially giving rise to a second generation of merged BHs (Rodríguez et al. 2018). Multiple-generation BBH mergers are likely within galactic nuclear clusters irrespective of the magnitudes of the BHs’ spins, where the escape speeds are large ($\gtrsim 100 \text{ km s}^{-1}$). These cases are beyond the scope of this paper.

the GW background noise for the PTA and the LISA. In the present work, among all the relativistic interactions that occur inside the model clusters, only the GR coalescences and the GR-slingshot interactions (see above) will be considered and a broader study will be presented in a future paper.

The straightest way to determine the innermost configuration of a hierarchical, compact subsystem, hosting a BBH or another type of compact-binary merger, is to print the Chain members directly from the NBODY7 subroutine `AR-chain/chain.f` with name `CHAIN` that contains the ARC algorithm (called as a separate subroutine from `CHAIN`). Currently, this is done when a Chain, that is passed through the `CHAIN` routine, contains more than two members (see below), at least one bound pair, and requires PN modification (as indicated by the PN-order indicator $IPN \geq 1$) of the lowest order or above (see above). Distinction is made between the cases when there is at least one Chain member that is bound w.r.t. the innermost binary and when all other Chain members are unbound w.r.t. it, which are recorded against the N-body time in separate (machine-readable, text) files. It is the latter record that identifies the GR-slingshot events. In both cases, the member masses, semi-major-axis, and eccentricity (m_1, m_2, a, e) of the innermost binary are recorded; in the bound case, the nearest bound orbit w.r.t. the binary (m_0, a_0, e_0) and as well the corresponding KL period, T_{KL} , are entered into the same record. When all the Chain members are unbound w.r.t. the binary (see above), information regarding the binary’s closest fly-by member (its mass, stellar type, parameters for the relative hyperbolic trajectory) is stored instead.

However, this alone is not sufficient since the Chain membership of a hierarchical configuration depends on the degree of its hierarchy. Especially, from the point of view of the difference in dynamical timescales of the innermost binary and of the outer members gravitationally bound to it, additional hierarchy is introduced when the innermost binary becomes relativistic (say, by gaining a high eccentricity due to its interactions with the outer, bound members), shortening the binary’s orbital-evolutionary timescales due to the associated PN modifications (*e.g.*, GR precession and GW-radiation shrinking of its orbit). In such cases, even for a nearly democratic triple (outer-periastron/inner-apoastron ~ 1), often, only the two members of the innermost (relativistic) binary comprise the Chain, and the third member becomes a part of the binary-Chain’s perturbors (there can, of course, be additional bound and unbound perturbors of the Chain). As can be seen from such a PN inner binary’s perturber outputs (see below), the number of its perturbors oscillate between zero and finite (typically, between 0 and 1 close to a coalescence) over a very small fraction of an N-body time (\sim the cluster’s dynamical time), as the outer, bound member(s) exit and enter the binary’s radius of gravitational influence. In fact, typically, when such a PN binary is marked as “COALESCENCE”, following one of the coalescence conditions in the `CHAIN` routine, the number of its perturbors is zero despite having bound outer members, meaning its GR-inspiral timescale (according to orbit-averaged PN-2.5; Peters 1964) has become short enough that it can be traced unperturbed up to coalescence (see, *e.g.*, Fig. 7 of Banerjee 2018) before the binary can again be perturbed significantly by an outer orbiter, justifying the “COALESCENCE” tag. However, although found more rarely in the

present computations, GR coalescence also happens within a Chain with > 2 members, in which case the innermost triple/multiple configuration, hosting the merger, can be obtained directly from the `CHAIN` outputs arranged as described above.

Therefore, in addition to recoding the Chain members as they are passed through the ARC routine, it is important to simultaneously scan and record members from the Chain’s perturber list. A new subroutine, currently named `BBHNB`⁵, which is also called from within `CHAIN`, executes this task by utilizing the handy `CHAINC` common block that contains information on the currently-executed Chain’s center of mass (hereafter COM) and the list of the identities of its perturbors. By following a similar procedure as in the default routine `GPU2/bhp1ot.f`⁶, `BBHNB` records (against the N-body and physical times; in machine-readable, text format) the masses, semi-major-axes, and eccentricities of up to five nearest (in the order of increasing semi-major-axis; the nearest one being denoted by m_0, a_0, e_0) bound perturbors of the Chain. The room for five bound neighbours is kept for just in case: hierarchies beyond triple are rare throughout the present model computations. In the case of a binary-Chain (see above), the mass and the orbital parameters of the innermost (Chain) binary ($m_1 + m_2, a, e$) and as well the T_{KL} w.r.t. the nearest bound perturber (if at least one bound perturber exists) are entered into the same record. Since, as found in the models in Table 1, such computed models can produce long-lasing, hierarchical triples, care should be taken *not* to print, particularly the `BBHNB` records, on every call of `CHAIN`, to avoid producing excessively large output files⁷.

2.3.2 Extracting model snapshots and its binary population

Apart from tracking compact subsystems, as described above, star-by-star snapshots of the “cluster” part of the stellar system (*i.e.*, of the stellar population within the instantaneous tidal boundary that is gravitationally self bound but for the on-the-way escapers) are obtained from the computed evolutionary models (Table 1) in intervals of 10 or 20 Myr. It becomes much more convenient to track specific stellar or binary type if the cluster data bank, as stored in the NBODY7’s default runtime output file `OUT3` in the binary data format (double precision for floating variables), is enhanced: apart from the N-body time, identities, masses,

⁵ As opposed to what the subroutine’s name, which is due to historical reasons, may indicate, this routine deals with *any* Chain that is passed through `CHAIN` and not just those which contain a BBH and/or are relativistic.

⁶ This procedure has been partly sketched in the “Discussion session on perspectives of NBODY6/7 with Sverre Aarseth” during the MODEST17 conference in Prague; see <ftp://ftp.ast.cam.ac.uk/pub/sverre/discuss.pdf>

⁷ This would affect the print-output cadence from `CHAIN` and `BBHNB`, so that a high-time-resolution recording of the subsystem evolution is currently prevented. Another parameter affecting the cadence of the subsystem output is the regularized time step parameter which is taken to be $\text{ETAU} = 0.1$ in the present computations. At present, the output cadence from `CHAIN` and `BBHNB` is increased with the PN order of the innermost Chain binary.

and the Cartesian components of positions and velocities, the BSE stellar-evolutionary stage (Hurley et al. 2000) of each star is also entered in every record (two N-body times apart). Each such snapshot is then searched for the closest gravitationally-bound pairs to retrieve the binaries (the members’ identities, masses, stellar types, derived orbital parameters, COM coordinates and velocities) at the corresponding evolutionary time. That way, the recovery of the binary population does not depend on the chosen KS regularization parameters (RMIN and DTMIN) and, in principle, all binaries, including those at the hard-soft limit (Heggie & Hut 2003), are obtained. Utilizing the stellar types, the binaries in a given snapshot can then be sorted for specific types such as star-star, BBH, BH/NS-star, BH/NS-MS, etc and utilizing the identity values the evolution of a given pair can be followed over the snapshots, through machine reading.

3 RESULTS

In this section, various aspects of the model computations in Table 1 are described.

3.1 In-cluster, general-relativistic coalescences driven by compact subsystems

As already shown in Papers I & II and found true as well for the broader set of models evolved here, the GR coalescences in young massive- and open-range clusters take place primarily inside the clusters, driven by the short-timescale, few- N dynamics of dynamically-formed compact subsystems (see Sec. 1) that are composed of one or more of the retained stellar remnants, typically of BHs. The newly arranged live tracking system of Chain subsystems, as described in Sec. 2.3.1, facilitates the recovery of the subsystems hosting the GR coalescences.

Fig. 1 depicts the configurations of (a subset of ⁸) the triple subsystems, formed dynamically in the computed models, in which the inner compact binary has undergone a GW-radiation inspiral and merger. The horizontal axis of Fig. 1 represents the hierarchy of the triple, as measured by the ratio, $\mathcal{R} \equiv a_0(1 - e_0)/a(1 + e)$, of the periastron of the outer orbit to the apoastron of the inner orbit and the vertical axis

represents the triple’s secular KL time period, T_{KL} (N-body units), given by (Kiseleva et al. 1998)

$$T_{\text{KL}} = \frac{2P_0^2}{3\pi P} (1 - e_0^2)^{3/2} \frac{m_1 + m_2 + m_0}{m_0}, \quad (1)$$

where P and P_0 are the Keplerian periods of the triple’s inner and outer orbits respectively. Note that the configurations in Fig. 1 correspond to a time very close, $\lesssim 10^{-4}$ N-body times, to the commencement of the GW inspiral of the inner binary (see Sec. 2.3.1). Therefore, the inner eccentricity, e , used in the definition of \mathcal{R} is the maximum inner eccentricity reached by the triple before the commencement of the inspiral.

Given that the majority of the configurations in Fig. 1 have $1 \lesssim \mathcal{R} \lesssim 10$ (full range $10^{-1} \lesssim \mathcal{R} \lesssim 10^2$), the triples, that ultimately drive the inner binary into coalescence, typically range from being marginally stable to stable. The typical range of their secular time period is $10^{-2} \lesssim T_{\text{KL}} \lesssim 10$ N-body unit (full range $10^{-4} \lesssim T_{\text{KL}} \lesssim 10^3$ N-body unit) and there is an overall positive trend between \mathcal{R} and T_{KL} . However, except for a few of those with the shortest T_{KL} s, these triples typically appear and remain in the clusters for time spans much shorter than their respective T_{KL} s, before the merger of the inner binary. Therefore, essentially all of these inspirals are triggered via chaotic (non-secular) interactions between the innermost (PN) binary and its (nearest) outer companion, that results in a rapid eccentricity growth of the binary (Sec. 1), irrespective of the extent of the hierarchy (\mathcal{R}); see also Antonini et al. (2016) in this context. Based on the CHAIN and BBHNB outputs (Sec. 2.3.1), the typical duration of the “final” triple that has led to a merger is a fraction of an N-body time (the dynamical time of the cluster). As can be expected, given the moderate to low velocity dispersion of the cluster environment and the fact that a triple, often composed of BHs (see below), would be the most massive compact-subsystem member in the cluster, the triple would be susceptible to significant alteration or destruction due to its dominant gravitational focusing. Therefore, it is unlikely to have the chance of undergoing many cycles of secular oscillations (Katz et al. 2011; Lithwick & Naoz 2011), and any dramatic outcome (*e.g.*, GR merger, high-velocity breakup), as a result of the triple evolution, would happen only due to its chaotic part (as obtained via a full 3-body integration such as the ARC; see Sec. 2.3). Like the secular Kozai-driven mergers (*e.g.*, Liu & Lai 2017; Antonini et al. 2018), one may plausibly expect that the mergers driven by such chaotic triple interactions would also exhibit spin-orbit misalignment, as hinted in at least one of the LIGO detections (Abbott et al. 2017a; Farr et al. 2017), although it deserves a dedicated study.

In fact, in the few cases of relatively long-term (at least for a few N-body times) Chains leading to a merger, it is also ambiguous to identify a single triple leading to the event. In these cases, a given inner binary have had its outer companion exchanged multiple times before its merger. Well before the merger, such binaries would also have more than one perturbers bound to it; although *rarely*, this is true for the short-term (< 1 N-body time) merger Chains too. However, except for one (which turns out to be a hierarchical quadruple), the final configuration of all the mergers shown in Fig. 1 is a triple, *i.e.*, the merging binary has only one orbiter. In a few cases (see below), this final outer member is actually a binary, *i.e.*, the final configuration hosting the

⁸ The developments in the CHAIN routine, as described in Sec. 2.3.1, have been implemented over time, in parallel to ongoing computations. The latest developments were available only to the most recent runs which explored the models with relatively low $M_{cl}(0)$ and high $f_{\text{bin}}(0)$. In the runs where both the direct CHAIN and the BBHNB outputs are available, making detailed extraction of the Chain-subsystem configurations possible, the corresponding entry in the N_{sling} column in Table 1 shows a value, otherwise a ‘-’ is shown. During the $M_{cl}(0) \approx 5.0 \times 10^4 M_{\odot}$ models’ computations, only a part of the direct CHAIN output arrangement was available, allowing the recovery of 4 of the triple configurations hosting GR mergers, from these models. One of the triple configuration, very close to the merger, could be obtained from the default Kozai output data. These 5 points are also included in Figs. 1 & 2. The rest of the runs in Table 1, although couldn’t be utilized for the purposes of the Secs. 3.1 & 3.2, are still utilized for the study of BH—non-BH binaries presented here (Sec. 3.4).

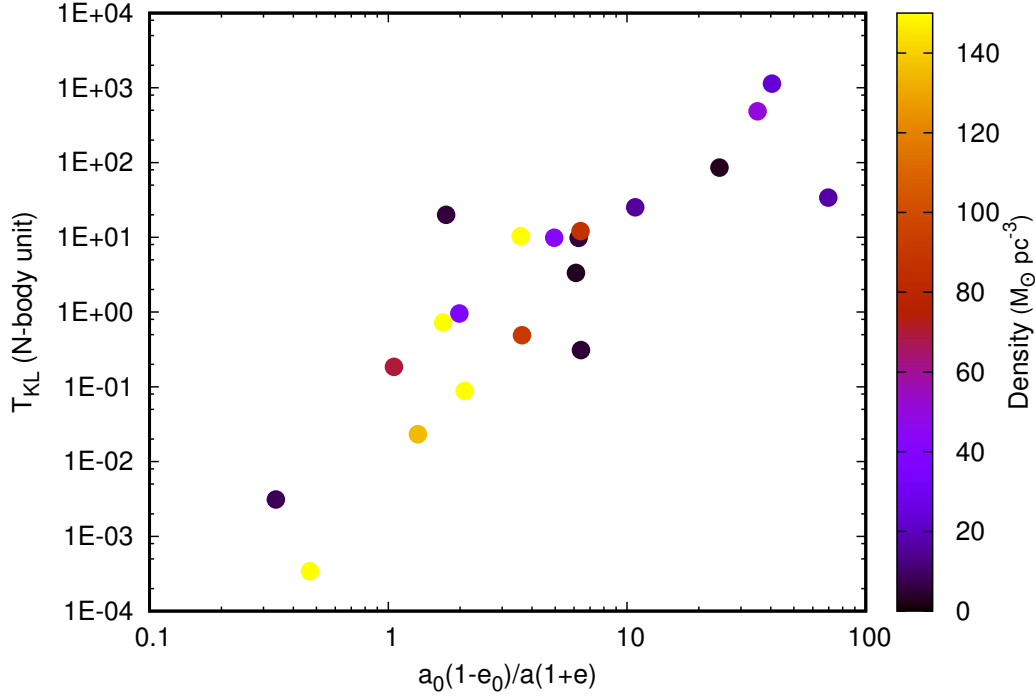


Figure 1. The configurations of the (innermost) triple subsystems hosting (a subset of) the GR BBH (and other types of compact-binary; see Sec. 3.1) coalescences, that occurred inside the computed cluster models in Table 1. The abscissa represents the ratio of the outer periastron to the inner apoastron of the triple, which measures the extent of hierarchy in the triple configuration. The ordinate represents the Kozai-Lidov timescales (N-body unit), T_{KL} , of these triples. These triple configurations correspond to times very close to the commencement of the GW inspirals of the inner binary (see Secs. 2.3.1 & 3.1). The colour coding (the colour bar) represents the mean density within the innermost 10% Lagrangian radius of the host cluster at the time of the coalescence, representing the environment in which the merger event has taken place.

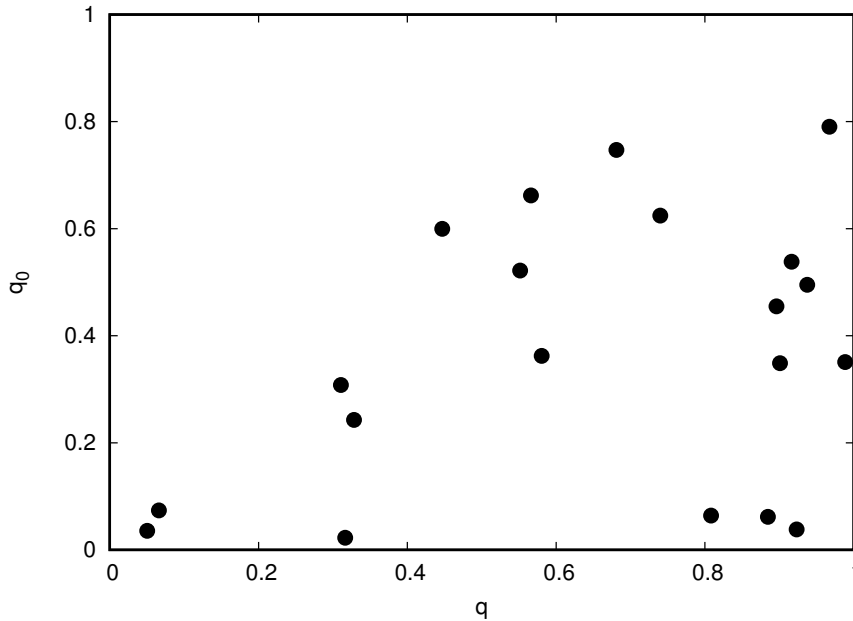


Figure 2. The mass ratios corresponding to the triple-hosted GR coalescences that are shown in Fig. 1. The mass ratio, q , of the inner, merged binary is plotted along the abscissa and that of the outer binary, q_0 , between the inner binary's total mass and the outer member's mass, is plotted along the ordinate.

merger is actually a binary-binary quadruple. Only one of the mergers (not shown in Fig. 1) happened following a GR slingshot (see Sec. 2.3, below). Clearly, a wide variety of dynamical interactions inside open clusters, involving a wide variety of compact subsystems (also, see below), lead to GR coalescences in them, which, perhaps, deserves a classification. This will be undertaken in a future study with a larger collection of merger events.

The colour coding in Fig. 1 (colour bar), which is according to the mean density within the innermost 10% Lagrangian radius of the host cluster at the time of the coalescence, represents the stellar density of the environment in which the merger has taken place. The qualitative trend in colour indicates that in higher-density environments, the GR mergers tend to take place in tighter (less hierarchical) triples: such tighter triples may exist in lower-density environments too but the reverse is unlikely. This is expected since a more crowded environment is more likely to clobber a triple with a looser outer member.

Fig. 2 shows the inner-binary vs. outer-binary mass ratio (q and q_0 respectively) of the mergers shown in Fig. 1. Most of the mergers are of (inner) BBHs having $0.2 \lesssim q \lesssim 1.0$ with the majority of them having $q \gtrsim 0.5$, as can be expected for mergers of dynamically-assembled BBHs (*c.f.* Fig. 6 of Paper II). The two mergers with $q < 0.1$ in Fig. 2 are BH-NS and BH-white dwarf (hereafter WD); although rare, such BH–non-BH GW-inspiral mergers do occur in these model computations which events would be accompanied by electromagnetic signatures (Abbott et al. 2017c)⁹. The outer members for these two mergers are also WDs (also, see below), as indicated by their small ($q_0 < 0.1$) values.

The outer members corresponding to most of the mergers in Fig. 2 are also BHs, making their q_0 s spread around 0.5. The ones with $q_0 \approx 0.8$ have a BBH, instead, as the outer member, *i.e.*, the subsystem configuration, just before the merger, is a BBH-BBH quadruple. The few mergers with $q_0 < 0.1$ have a non-BH outer member.

3.2 General-relativistic “slingshot” interactions inside clusters

As already pointed out in Sec. 2.3, temporarily PN binaries are found to appear *inside* the computed models due to close fly-by interactions between a compact binary and a single object. These binaries, although unlikely to undergo GW inspiral (see Sec. 1), would nevertheless be interesting as they, among others (*e.g.*, temporarily-relativistic triples), would potentially contribute to the low-frequency GW noise flux from the cluster. Fig. 3 shows such GR slingshots which occurred inside a subset of the computed model clusters in Table 1. As recovered from the direct CHAIN output (Sec. 2.3.1), these are Chains containing only one PN binary and the rest of the Chain’s members (typically one)

are unbound w.r.t. it, indicating a close, fly-by encounter with the binary that has imparted a high eccentricity onto it, making it PN. In Fig. 3, the peak-power frequency of the broadband GW emission of such eccentric binaries, as given by the expression (Wen 2003)

$$f_{\text{GWP}} = \frac{\sqrt{G(m_1+m_2)}}{\pi} \frac{(1+e)^{1.1954}}{[a(1-e^2)]^{1.5}}, \quad (2)$$

is plotted against the host cluster’s evolutionary time. This reasonably assumes that the binary passes through its periastron at least a few times before it is altered again by the next significant encounter.

As the corresponding chirp masses (color coding in Fig. 3) defined as

$$M_{\text{chirp}} \equiv \frac{(m_1 m_2)^{3/5}}{(m_1 + m_2)^{1/5}} \quad (3)$$

indicate, the majority of these GR-slingshot binaries are BBHs although a few of them are WD-WD, BH-WD, and BH-MS. Note that such close, fly-by, binary-single interactions would show up in CHAIN around their closest separations, essentially extracting the configuration of the participants of the interaction over the small time interval during which the slingshot happens, which is what are plotted in Fig. 3. The binary can thereafter be followed from the direct CHAIN outputs: a more elaborate study of these GR-slingshot binaries plus other instances of temporarily-relativistic systems that appear within the clusters will be undertaken in a forthcoming work.

As seen in Fig. 3, around half of the detected slingshot binaries fall in the LISA’s characteristic detection-frequency band, which would then, in principle, serve as persistent sources for the LISA. The rest of them, here, primarily fall in the gap between the characteristic detection bands of the LISA and the PTA with a few but one of them marginally entering the PTA band. Note that the GR-slingshot binaries are, generally, highly eccentric ($1-e < 0.1$), that would make their “proper” detection including their orbital parameters questionable. However, they would still contribute to the GW background for these instruments.

The GR slingshots tend to occur more frequently over $t \lesssim 1$ Gyr cluster-evolutionary time due to the generally larger number of BHs present in the clusters over their initial evolution.

3.3 The ambient binary black hole population inside clusters

BBHs continue to form, dissociate, and get ejected via dynamical interactions from within the clusters’ innermost regions where the density of the BH population is the highest due to their segregation via dynamical friction (Kulkarni et al. 1993; Sigurdsson & Hernquist 1993). The two main dynamical channels of BBH formation are (a) binary formation via 3-body gravitational interactions (Heggie & Hut 2003) among single BHs and (b) multiple exchange interactions of single BHs with stellar binaries. In the presence of a substantial population of primordial binaries, a population of BBHs derived from the (dynamically-modified) evolution of massive primordial binaries can also be expected inside the clusters.

⁹ Among the merger events shown in Figs. 1 & 2, the BH-NS one has happened in the computation with the speed of light $c/100$ (Table 1). However, the BH-WD merger here and also the BH-NS merger identified in one of the models in Paper II (not shown here due to the unavailability of the subsystem data; see above, Table 1) have occurred in models where the physical speed of light has been used.

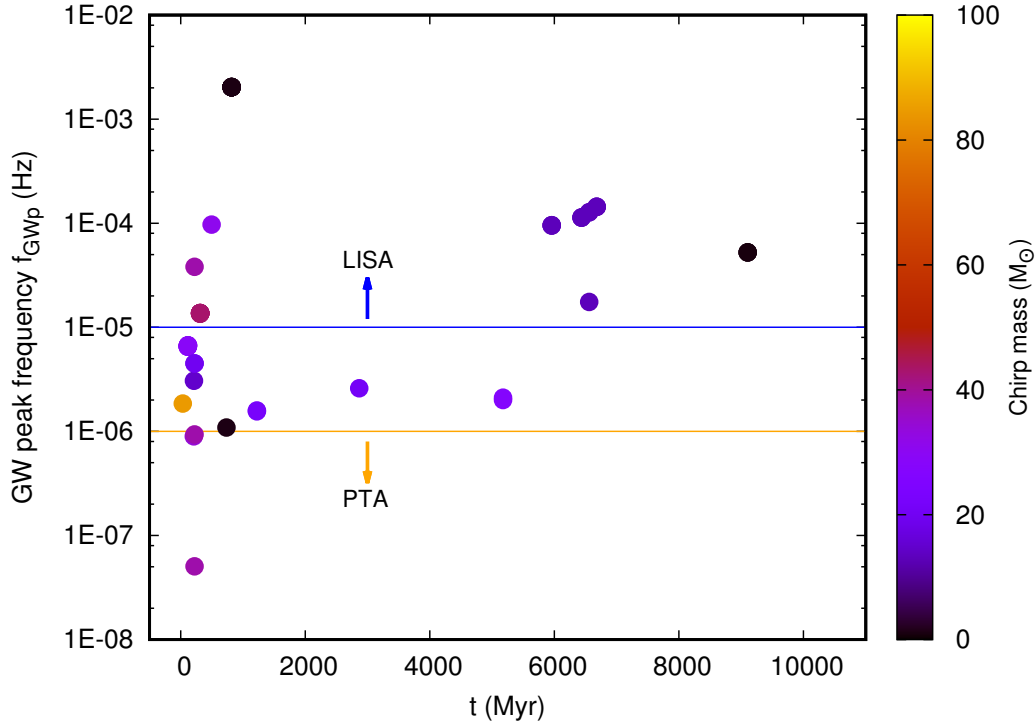


Figure 3. The peak-power GW frequency, f_{GWp} (ordinate), during the “GR slingshot” interactions recorded by (a subset of) the computed models (Table 1). The abscissa represents the host-cluster-evolutionary time, w.r.t. a common $t = 0$, of the occurrence of these interactions and the colour coding represents the chirp mass, M_{chirp} , of these “temporarily-relativistic” binaries. Although the majority of such binaries are BBHs, some of them are also BH-non-BH and non-BH-non-BH. The characteristic frequency bands for the LISA and the PTA are indicated; although such interactions did not result in complete GR inspirals, they would still potentially give rise to temporary sources for the LISA.

Figs. 4 and 5 show the BBHs bound to the evolutionary model clusters with $M_{cl}(0) \approx 1.5 \times 10^4 M_{\odot}$ and $3.0 \times 10^4 M_{\odot}$ respectively with varying Z and $f_{\text{bin}}(0)$. Figs. 6 and 7 show those for the models with $f_{\text{bin}}(0) \approx 0.05$ and $f_{\text{bin}}(0) \approx 0.5$ respectively with varying $M_{cl}(0)$ and Z . In a particular panel, the semi-major-axes (limited to $a < 1000$ AU) of all the BBHs present in the corresponding model cluster’s snapshot at the evolutionary time t (filled squares, colour coded with the total BBH mass), recovered as described in Sec. 2.3.2, are plotted against t . In Fig. 8, the eccentricities of the BBHs inside four of the models are similarly demonstrated and in Fig. 9, the BBHs’ radial distances from the cluster’s density center are plotted for these four models.

A continuous trail of points, several of which per panel can be easily noticed in these figures, represents the evolution of a particular BBH. In general, two categories of BBHs exist in a cluster. Over the earliest evolutionary times ($t \lesssim 1$ Gyr), the in-cluster BBH population of a sub- Z_{\odot} cluster is dominated by those that are derived from massive primordial binaries whose original members continue to remain paired even after they are evolved into BHs (in NBODY7 models, such BBHs necessarily have members with consecutive identity numbers). These can be noted as the near-horizontal trails in Figs. 4, 5, 6, 7. These BBHs typically have widths $10 \lesssim a \lesssim 100$ AU and total masses $M_{\text{tot}} \lesssim 40 M_{\odot}$ (with a few of them being of $40 M_{\odot} \lesssim M_{\text{tot}} \lesssim 60 M_{\odot}$). A larger number of such primordial-binary-derived (but potentially dynamically-modified) BBHs are initially present in models

with higher $f_{\text{bin}}(0)$, higher $M_{cl}(0)$, and lower Z : massive binaries comprising members of lower Z widen to a less extent due to less mass loss in stellar winds and produce more massive (direct-collapse) BHs, resulting in tighter BBHs that are less susceptible to dynamical dissociation inside a dense environment (Morscher et al. 2015; Chatterjee et al. 2017a). The combination of their tightness, relatively lower mass (hence, weaker gravitational focussing), moderate eccentricities, e (see Fig. 8), and, most importantly, generally outer-region location (see Fig. 9) where the stellar density is low would cause them to undergo close interactions rarely and hence to encounter-harden (Heggie 1975) very slowly, mostly via distant, weak encounters. Although the massive, O-star binaries (see Sec. 2.1), that would potentially evolve into such BBHs, would sink to the cluster’s center via dynamical friction within a few Myr, a fraction of them can get ejected from the central region to the outer parts of the cluster (but without getting altogether unbound from the cluster) via dynamical encounters over a similar period due to the concentration of the most massive entities within the innermost region. Additionally, the wind mass loss from such a dynamically-kicked massive binary, which is still substantial at low Z (according to Vink et al. 2001 as adopted here; see Paper I), would further drive it into outer orbits, apart from widening it at the same time. Admittedly, the presence and the properties of such primordially-paired BBHs would depend on the choice of the primordial massive-binary population (Sec. 2.1).

In contrast, the dynamically-formed BBHs (recognizable by non-consecutive member identities) begin to appear from $t \gtrsim 100$ Myr with generally much wider $a \gtrsim 100$ AU and higher e (Fig. 8) and much more centrally (Fig. 9), enabling them to intercept encounters much more frequently and undergo encounter hardening efficiently (Banerjee & Ghosh 2006, and references therein). These are the slant trails in Figs. 4, 5, 6, 7 (*c.f.*, Fig. 3 in Banerjee et al. 2010). As can be noted in these figures, in general, more massive dynamical BBHs appear and harden at earlier evolutionary times which is expected since the most massive BHs in the system would tend to pair up first and hence get dynamically processed earlier (Morscher et al. 2015; Chatterjee et al. 2017b; Banerjee 2018). The eccentricities of these frequently-interacting BBHs alter widely with time, which is why it is difficult to locate such trails in Fig. 8.

However, at any given time, there is necessarily only a few dynamically-assembled BBHs existing in a cluster, irrespective of the cluster’s mass, stellar-binary fraction, and BH population. This is demonstrated in Fig. 10 where, on each panel, the time evolutions of the total bound BBH population and of the dynamically-formed BBH population are shown separately. The majority of both types of BBHs ultimately get ejected from the clusters via a close dynamical encounter, when the trails in Figs. 4, 5, 6, 7 terminate, typically at $a \sim 10$ AU, depending on the escape speed at the location of the encounter within the cluster (likely close to the cluster’s center) at the time of the ejection (Banerjee et al. 2010; Chatterjee et al. 2017a). In particular, for a given cluster and over similar cluster-evolutionary times, those BBHs that generally reside in the inner regions (mostly, the dynamically-formed ones) are hardened dynamically to tighter a s before getting ejected by a final encounter: that is why, as in, *e.g.*, Figs. 5 & 6, there are (more massive) BBHs that are being hardened efficiently, at early as $t \sim 100$ Myr, unlike most of the (primordially-paired) others that aren’t, over similar evolutionary times (*c.f.*, the corresponding panels in Fig. 9). The properties of such ejected BBHs are discussed in detail in Papers I & II. A few of them terminate by undergoing triple-induced GR coalescences as discussed in Sec. 3.1. As can be read from Figs. 4, 5, 6, 7, the characteristic lifetime of the primordially-paired BBHs is ~ 100 Myr and that for the dynamical BBHs is \sim Gyr.

3.4 Black hole-main sequence binaries inside clusters

At late evolutionary times, BH—non-BH binaries form in these model clusters exclusively via exchange interactions between BHs and normal stellar binaries. Since, motivated by observations, the BH-progenitor O-type stars are here paired separately (see Sec. 2.1), only BH—O-star binaries, that exist over the first ≈ 10 Myr, can be obtained from the initial pairings, among the BH—non-BH pairs in the cluster.

Fig. 11 demonstrates the evolution of the stellar-binary population in a representative set of the models from Table 1. As expected, the total number of binaries, $N_{\text{bin}}(t)$ (normalized w.r.t. the initial number of binaries, $N_{\text{bin}}(0)$; right column in Fig. 11), decreases monotonically with time as they get dissociated or ejected from the clusters due to dynamical interactions. The instantaneous binary fraction, $f_{\text{bin}}(t)$, decreases for the first 1-3 Gyr after which $f_{\text{bin}}(t)$ be-

gins to increase again (left column in Fig. 11). As the BHs deplete from a cluster due to encounters (see Fig. 10; Paper I), their dynamical heating weakens, aiding the stellar binaries to resume their mass segregation (see Papers I & II) via two-body relaxation. When, due to its expansion by BH and binary heating (see Papers I & II; Fig. 18), the cluster begins to get trimmed, through the tidal boundary, from its outer, lower-binary-fraction regions (as per the mass segregation of the binaries), the binary fraction within its remaining, bound part increases. The growth of $f_{\text{bin}}(t)$ is to a larger extent, closer the cluster is to its dissolution at the end of the computation, and can even exceed $f_{\text{bin}}(0)$ close to its disruption (see Fig. 11).

Figs. 12, 13, 14, and 15 show the BH-MS (filled circles) and NS-MS (filled squares) binaries ($a < 1000$ AU), in the $a-t$ plane, formed inside the computed model clusters of Table 1. Figs. 12 and 13 show the BH-MSs/NS-MSs inside the clusters with $M_{cl}(0) \approx 1.5 \times 10^4 M_{\odot}$ and $3.0 \times 10^4 M_{\odot}$ respectively with varying Z and $f_{\text{bin}}(0)$. Figs. 14 and 15 show those for the models with $f_{\text{bin}}(0) \approx 0.05$ and $f_{\text{bin}}(0) \approx 0.5$ respectively with varying $M_{cl}(0)$ and Z . In these figures, which are obtained from the computed models’ snapshots as described in Sec. 2.3.2, the points are colour coded according to the MS companions’ mass (at time t).

As seen in these figures, nearly all models produce intermediate- ($t \gtrsim 10$ Myr) and late-time ($t \gtrsim 1$ Gyr) BH-MS binaries (filled circles) of widths $a \sim 100$ AU. However, the high- $f_{\text{bin}}(0)$ and/or lower- Z models contain BH-MSs of $a < 1$ AU to $a \sim 100$ AU at times as early as $t \leq 10$ Myr, which are evolved pairs of massive stars from $t = 0$ (that may thereafter become BBHs derived from primordial pairs; see Sec. 3.3). As explained above, all the BH-MS binaries at intermediate and late times are necessarily dynamically assembled. Some of the models form tighter BH-MSs at intermediate and late times, of $a < 1$ AU to $a \sim 10$ AU, which are prospective candidates to be identified through radial-velocity measurements of the MS companion. Typically, these are the models that have high $f_{\text{bin}}(0)$ (> 0.3) or expand moderately or undergo contraction at late times (see Fig. 18) or have a combination of these properties, which favour exchange interactions of the BHs with the relatively tight stellar binaries. A few these tighter BH-MS binaries have their MS companion’s mass $\gtrsim 0.8 M_{\odot}$ (colour coding in Figs. 12, 13, 14, and 15), which makes them similar to the radial-velocity-identified (detached) BH-MS binary in the GC NGC 3201 (Giesers et al. 2018). The overall mass range of the MS companion in these dynamically-formed BH-MS binaries is, however, wide: from $\approx 0.1 M_{\odot}$ to $\gtrsim 1.0 M_{\odot}$.

Some of these models produce NS-MS binaries (filled squares in Figs. 12, 13, 14, and 15) which are generally wide, of $a \sim 100$ AU. Two of the NS-MSs are tighter with $a \sim 10$ AU (see top-right & bottom-left panels of Fig. 12). As pointed out in Paper II (see also Fragione et al. 2018), the BH heating keeps the NS population within a cluster so that the NSs, although comparable to or larger than the BHs in number, intercept lower-density environments in the cluster compared to the BHs where the chances of exchanging with a tight stellar binary is smaller (the two tight NS-MS binaries form in less-expanded and high-stellar binary fraction models).

The recent observations by Shishkovsky et al. (2018)

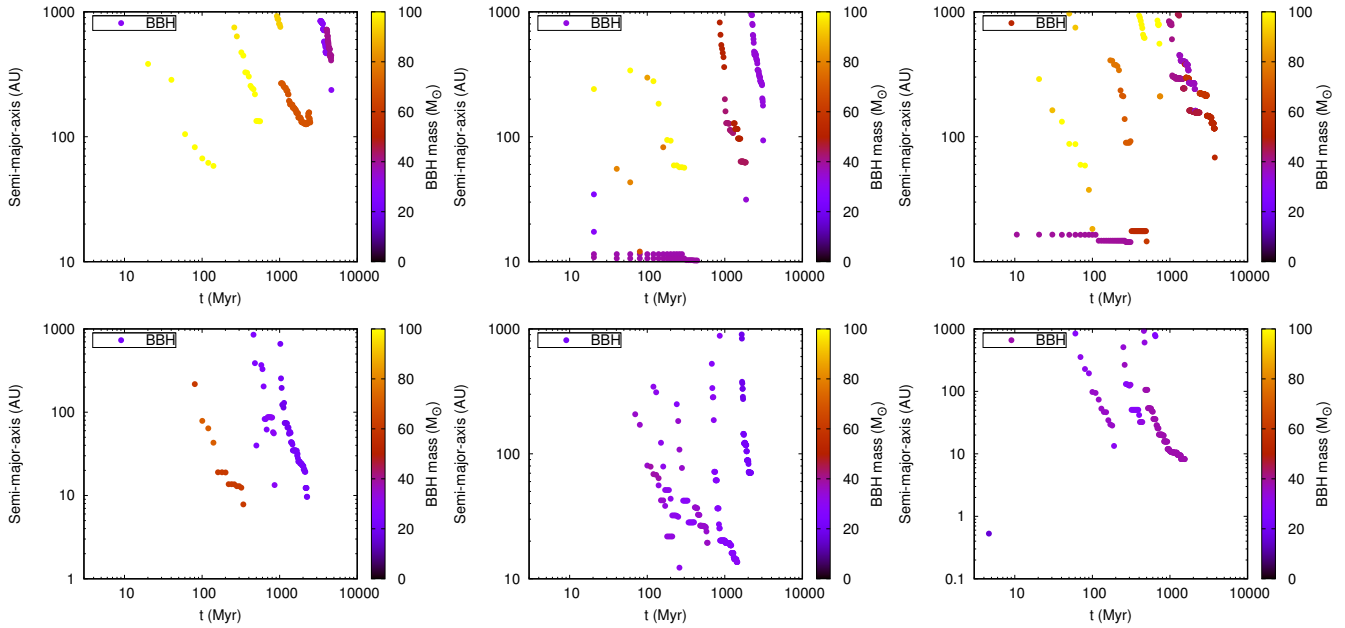


Figure 4. Binary black holes (BBH; filled circles) in the computed $M_{cl}(0) \approx 1.5 \times 10^4 M_{\odot}$ models with evolutionary time, t , as a function of increasing primordial binary fraction, $f_{bin}(0) \approx 0.05, 0.30, 0.50$ (left to right panels), and for metallicities $Z = 0.001$ (top panel) and 0.02 (bottom panel). On each panel, that represents a particular computed model, the vertical axis is the instantaneous semi-major-axes (< 1000 AU) of the BBHs that are bound to the cluster snapshot at time t . A continuous trail of points represents a specific BH-BH pair. The colour coding (colour bars) represents the total BBH mass. In this and the following Figs. 5, 6, 7, 8, 9, and 10, the “test” runs in Table 1, that include tidal interaction (Sec. 2.2), are excluded, which are presented separately in Fig. 19.

make it tempting to look for binaries in the computed models in which a BH or an NS is paired with a giant or an even more evolved stellar companion. Such binaries could be identified in a few of the models in Table 1 which are shown in Fig. 16. Here, such binaries containing BHs are formed with $a \sim 1 - 10$ AU. Also, those containing NSs are formed with $a \sim 10 - 100$ AU. None of these are, however, tight enough to be RLO, as may be the case with the BH candidate in Shishkovsky et al. (2018).

The lifetimes of the in-cluster BH-MS/BH—evolved-star binaries in Figs. 12, 13, 14, 15, and 16 are typically ~ 100 Myr; they cover a wide range of values from ~ 10 Myr (seen as a dot) to \sim Gyr. The same can be said for the NS binaries in these figures. These binaries either get dynamically ejected from the cluster or get their stellar member exchanged by an NS or a BH. Indeed, the \sim Gyr-long binaries are hosted only by the lower-mass clusters, where the chances of exchange or ejection are generally lower due to lower stellar densities and fewer numbers of NSs and BHs. Only a few BH-MS/BH—evolved-star binaries are ejected from the present models, taken together. Likewise the BBHs (Sec. 3.3), at most a few BH-MS retain in a cluster at a given time irrespective of the cluster’s properties or the BH population within it, as demonstrated in Fig. 17. Such sparsity of BBH/BH-MS/BH—evolved-star systems is also inferred in recent Monte Carlo studies of GC models (e.g., Arca Sedda et al. 2018; Askar et al. 2018).

All the BBH- and BH-MS—forming models discussed until now do not materialize the orbital energy dissipation due to tidal interactions which may influence binary orbits and aid in tightening dynamically-formed compact—

non-compact binaries and also potentially result in tighter double-compact binaries; see Sec. 2.2. A few relatively short duration test computations, with otherwise similar type of cluster models (Sec. 2), are performed with the tidal interaction activated (see Table 1). Fig. 19 shows the BBHs (upper panels) and the BH-MSs (lower panels) formed in these models. The BBHs exhibit similar properties as in the previous models. In two of these three models, very tight (< 1 AU) BH-MSs are formed well within 1 Gyr of cluster evolution that live for ~ 100 Myr and in the third model, several ~ 10 AU BH-MSs of similar longevity are formed within 1 Gyr. Compared to the frequency of occurrences of similarly-tight binaries in the previous models spanning a similar range of parameters, it then appears that the inclusion of tidal energy dissipation (which, currently, is implemented in NBODY7 according to Mardling & Aarseth 2001 which recipes are valid for low-mass MS stars only) may indeed help to form tighter BH-MSs, which will be investigated in detail in a forthcoming work. None of the models presented in this work, however, form a stable RLO binary: longer-term computations including tidal interaction may be the key to form them in model clusters (as in, e.g., Kremer et al. 2018b) which will be investigated in the near future.

3.5 Remark on the contribution from open clusters on the dynamical binary black hole merger rate

In Paper II, it has been shown, based on minimalistic estimates on BBH merger generation from young massive- and open-type clusters, that such clusters would collectively pro-

duce present-day (dynamical) BBH mergers at a rate comparable to that from the GCs (and hence to that from the nuclear clusters since the latter two can also be similar; see, Hoang et al. 2018). The key to this estimate (but see Sec. 3.3 of Paper II for the details) is the observationally-motivated (*e.g.*, Gieles et al. 2006; Larsen 2009) assumption that the progenitors of open clusters and GCs follow a power-law (cluster) initial mass function of index -2 and that the lower birth-mass limit of the merger-producing clusters is $M_{cl}(0) \approx 10^4 M_{\odot}$, inferred based on the computations in Paper II.

The set of model computations presented here extends down to $M_{cl}(0) \approx 7.5 \times 10^3 M_{\odot}$ which still produces BBH mergers, at least for high $f_{bin}(0)$ and low Z (see Table 1). Although, several models of $M_{cl}(0) \approx 5.0 \times 10^3 M_{\odot}$ has also been explored under various conditions, *e.g.*, with low and high $f_{bin}(0)$ and Z and also under solar-neighborhood-like and dwarf-galaxy-like external fields, no BBH or other types of GR coalescences, either in-cluster or ejected, could be obtained from them. Such models, however, can still be interesting for the production of temporarily-relativistic systems (Sec. 3.2).

Hence, based on the computations until now and given the adopted recipe for stellar-remnant retention (Sec. 2.2), if $M_{cl}(0) \approx 7.5 \times 10^3 M_{\odot}$ is plausibly taken to be the working lower mass limit of the progenitors of open clusters (*i.e.*, of young massive clusters) that would give rise to dynamical GR coalescences, then it only strengthens the conclusion that the young massive and open clusters would collectively produce present-day (dynamical) BBH mergers, visible by the LISA and the LIGO-Virgo, at a rate that is comparable to those from the GCs and the galactic nuclei.

4 SUMMARY

In terms of computed models' ingredients, a significant leap forward in the present work from its precursors, namely Papers I & II (Sec. 1), is the inclusion of high primordial binary fractions, $f_{bin}(0) \approx 30 - 50\%$, which takes these models closer to realistic massive open clusters (Sec. 2.1). Since long-term direct N-body computations (Sec. 2.3) of massive clusters with such high binary fractions is challenging, such $f_{bin}(0)$ is used for models with $M_{cl}(0) \lesssim 1.5 \times 10^4 M_{\odot}$; for the rest of the models, $f_{bin}(0) \lesssim 0.1$ is used (Table 1). Nevertheless, it is for the first time that the dynamics of stellar-mass BHs is studied ab initio in high-binary-fraction massive cluster models, through detailed and completely self-consistent relativistic direct N-body simulations. Another new aspect in this work is to be able to live-track in direct N-body simulations (Sec. 2.3.1), the configurations of the few-body subsystems that drive the GR mergers inside the massive clusters, for the first time. The key inferences based on the model computations of open clusters in this study are as follows:

- GR inspiral and coalescences occur inside young massive and open clusters with birth masses $M_{cl}(0) \gtrsim 7.5 \times 10^3 M_{\odot}$ (Table 1), under conditions that are realistic for such clusters, as long as a population of compact stellar remnants (NSs and BHs) are retained in the clusters at birth. Although the majority of such mergers are of BBHs, it is possible that other types of stellar remnants also participate in GR coalescences inside the clusters, *e.g.*, mergers of BH-NS

and BH-WD (Sec. 3.1). In addition to generating GW that is detectable by the LISA and LIGO-Virgo, the latter types of mergers would also generate electromagnetic imprints of the events. Young massive and open clusters would potentially contribute to present-day (dynamical) BBH mergers, visible by the LISA and the LIGO-Virgo, at a rate that is comparable to those from the GCs and the galactic nuclei (Sec. 3.5).

- The GR inspirals take place inside clusters via intricate dynamical interactions, that involve dynamically-assembled compact subsystems which are most often triples (Sec. 3.1). Such triples typically range from being marginally hierarchical to hierarchical in configuration (Fig. 1), although the onset of the GR inspiral of the inner binary and its merger would take place due to the chaotic interaction of the binary with its outer companion. Such GR-coalescence-hosting triples are typically composed of BHs although both the inner and the outer binary can, possibly, contain a non-BH member, *e.g.*, an NS or a WD (Fig. 2, Sec. 3.1). The subsystems leading to a GR merger can, possibly, be even more complex, *e.g.*, a relatively long lasting triple undergoing multiple exchanges of its outer member. The mergers can also take place within an even higher-order subsystem, *e.g.*, inside a quadruple (of both binary-binary and hierarchical configurations).

- A close, fly-by encounter between a purely Keplerian compact binary and a single member can impart sufficient eccentricity (plus any hardening) onto the binary so that it becomes PN, which interactions are termed here as ‘‘GR slingshot’’s (Sec. 3.2). As in the case of triple-mediated GR inspirals (see above), the participants of such encounters are mainly BHs but NS, WD, and MS stars can also take part. Approximately half of such GR-slingshot binaries have their peak-power GW frequency in the LISA’s characteristic detection band and a few of them also fall in the PTA’s band (Fig. 3); that way a population of such binaries in the stellar clusters of the Milky Way and the other nearby galaxies would potentially contribute to the GW background noise for the LISA and the PTA. However, such fly-by interactions, which predominantly take place over the first \sim Gyr of the host clusters’ evolution, rarely lead to full GR inspiral and coalescence of the GR-slingshot binaries.

- Intermediate-aged and old open clusters harbour detached BH-MS binaries that continue to form and destroy in (get ejected from) them via exchange (close) encounters (Sec. 3.4; Figs. 12, 13, 14, 15, 19). Such clusters also contain detached NS-MS binaries and also BH/NS paired with evolved stellar companions (Fig. 16). In clusters that are relatively dense and contain high stellar binary fraction at late times, a few BH-MS binaries are formed tight, with $a < 10$ AU, which are good candidates to be identified in the open clusters through radial-velocity measurements of the MS companion, as in the case of the GC NGC 3201. The BH—evolved-star companions, when formed, and, more rarely, the NS-MS binaries are also similarly tight. The BH/NS—MS/evolved-star binaries typically last for ~ 100 Myr, before getting the MS companion exchanged by a BH/NS or getting dynamically ejected from the cluster, although they would last up to \sim Gyr in lower-density environments. Although the present models have produced detached BH-MS binaries with properties consistent to the one identified in NGC 3201 (Giesers et al. 2018), open clusters would potentially

harbour a wide range of remnant—normal-star binaries with prospects of discovery via forthcoming radial-velocity surveys.

- Throughout their evolutionary times, young massive and open clusters harbour a population of BBHs that continue to form, get modified, get ejected or undergo GR coalescences via dynamical interactions (Sec. 3.3; Figs. 4, 5, 6, 7, 19). The BBHs which maintain the primordial pairings at their appearance are typically found in relatively low-density outer regions of the clusters (Fig. 9) where they undergo gradual orbital decay via weak encounters (that would accelerate only after they sink, via dynamical friction, further into the cluster, where the stellar density is higher). In contrast, the dynamically-assembled BBHs, which are also typically more massive and initially wider, are assembled in the innermost region of the cluster where they can undergo dynamical hardening efficiently, owing to the much higher stellar density and the prominence of BHs. Irrespective of a cluster’s parameters (*e.g.*, its mass, binary fraction) and the BH population contained in it, the ambient number of BBHs and BH-MSs within it is always a only few (Secs. 3.3 & 3.4; Figs. 10 & 17).

ACKNOWLEDGEMENTS

SB is thankful to the anonymous referee for constructive comments which have helped to improve the presentation of this work. SB is indebted to Sverre Aarseth of the Institute of Astronomy, Cambridge, for his efforts in improving NBODY6/7, without which this study would not have been possible. This work has been partly supported by the Deutsche Forschungsgemeinschaft (DFG; German Research Foundation) through the individual research grant “The dynamics of stellar-mass black holes in dense stellar systems and their role in gravitational-wave generation” (BA 4281/6-1; PI: Sambaran Banerjee). An enhanced version of the `Fortran` routine `OrbitDat`, originally written by Pavel Kroupa and Ladislav Subr, has been utilized in this work. SB is thankful to the computing team of the Argelander-Institut für Astronomie, University of Bonn, for their efficient maintenance of the workstations on which all the computations have been performed.

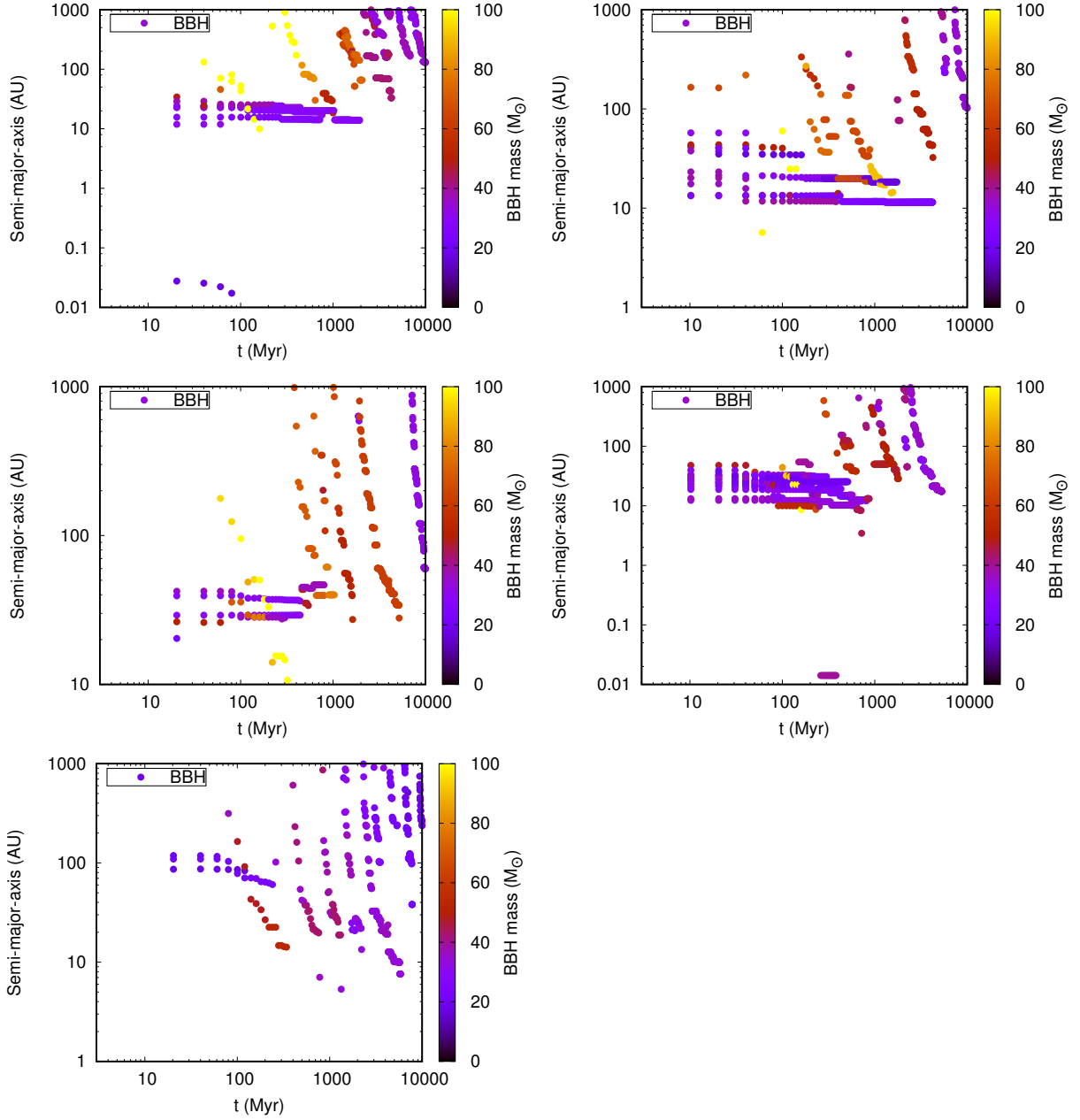


Figure 5. The BBH content in the computed $M_{cl}(0) \approx 3.0 \times 10^4 M_{\odot}$ models with evolutionary time, t , as functions of increasing primordial binary fraction, $f_{\text{bin}}(0) \approx 0.05$ (left), 0.10 (right) and metallicity $Z = 0.001$ (top), 0.005 (middle), and 0.02 (bottom). The legends are the same as in Fig. 4.

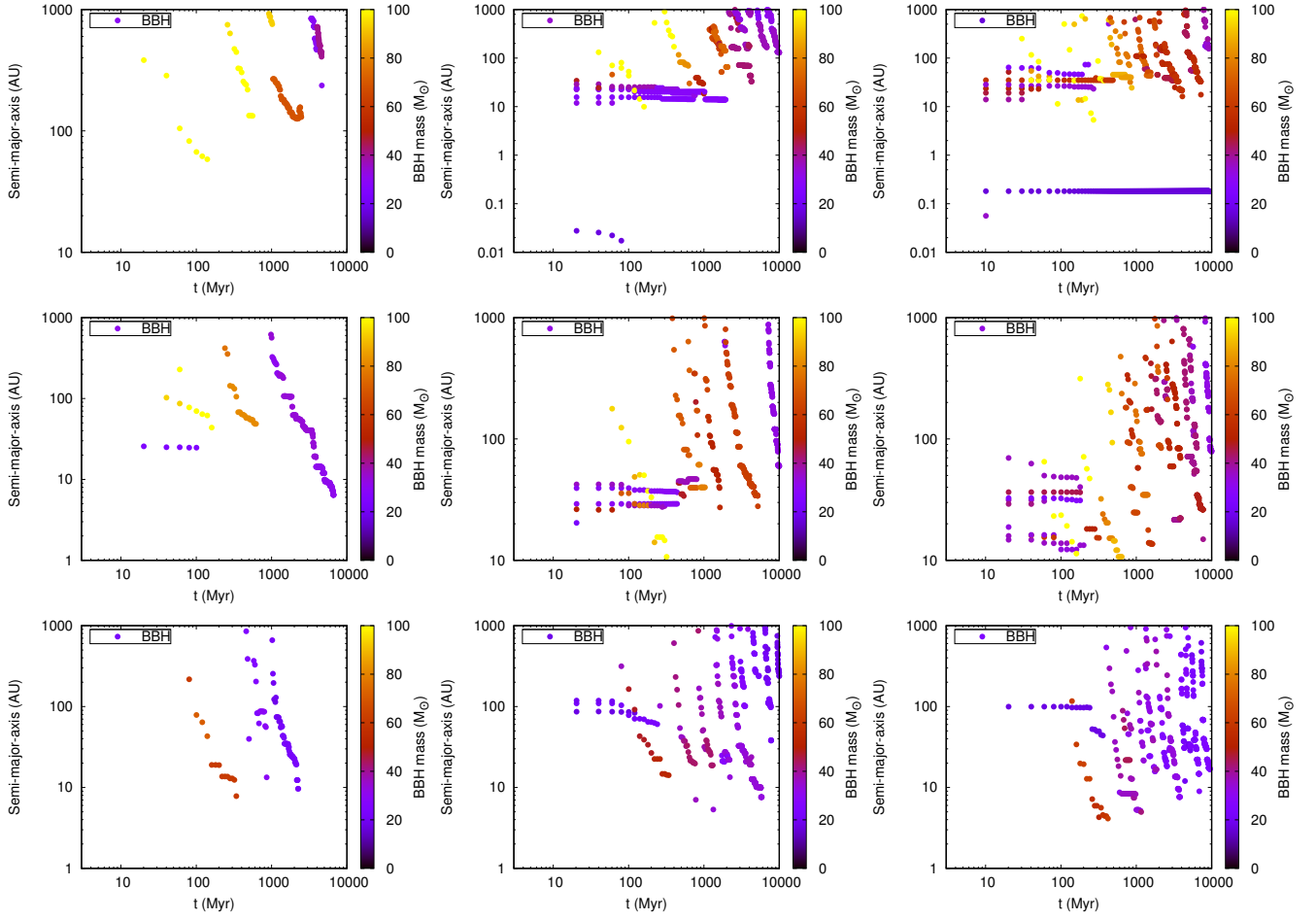


Figure 6. The BBH content in the computed $f_{\text{bin}}(0) \approx 0.05$ models with evolutionary time, t , as a function of increasing $M_{cl}(0) \approx 1.5 \times 10^4 M_{\odot}$, $3.0 \times 10^4 M_{\odot}$, $5.0 \times 10^4 M_{\odot}$ (left to right) and $Z = 0.001, 0.005, 0.02$ (top to bottom). The legends are the same as in Fig. 4.

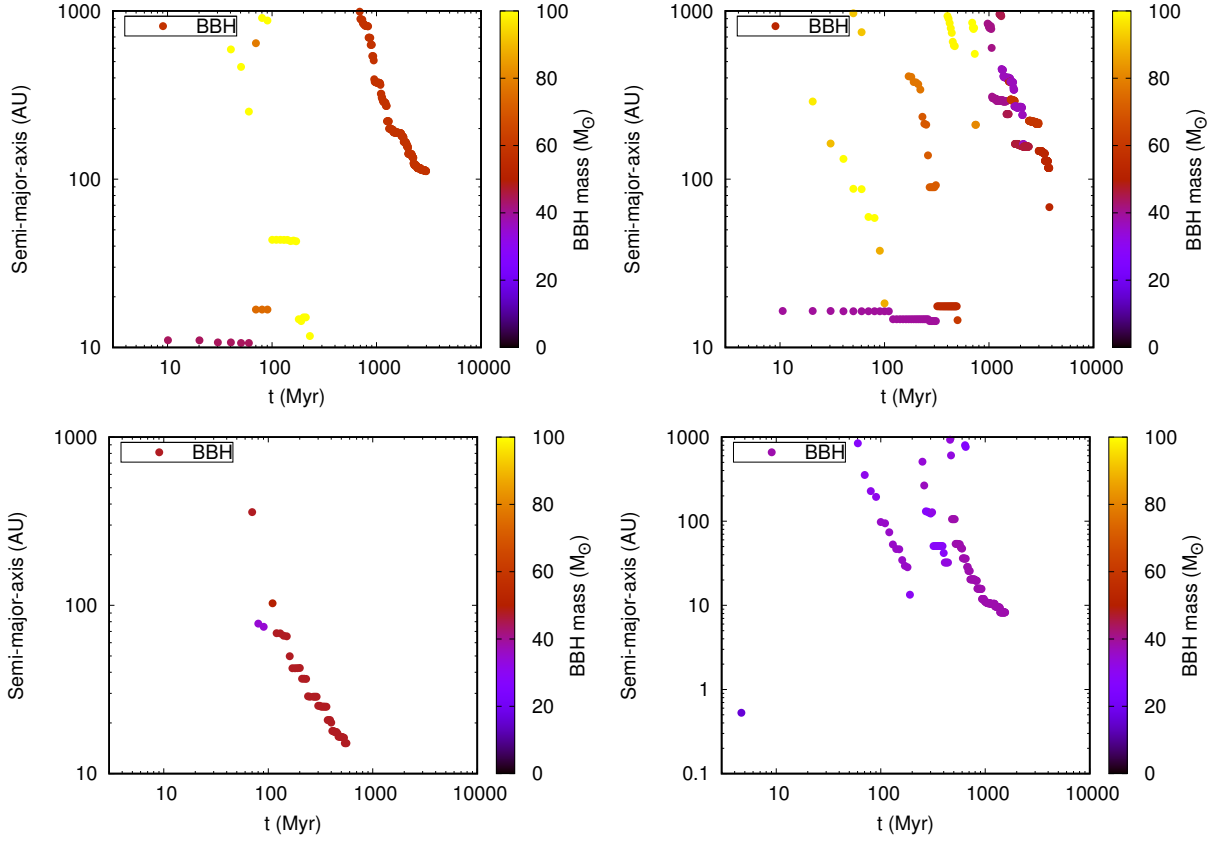


Figure 7. The BBH content in the computed $f_{\text{bin}}(0) \approx 0.50$ models with evolutionary time, t , as a function of increasing $M_{cl}(0) \approx 7.5 \times 10^3 M_{\odot}$ (left) and $1.5 \times 10^4 M_{\odot}$ (right) and for metallicities $Z = 0.001$ (top) and 0.02 (bottom). The legends are the same as in Fig. 4.

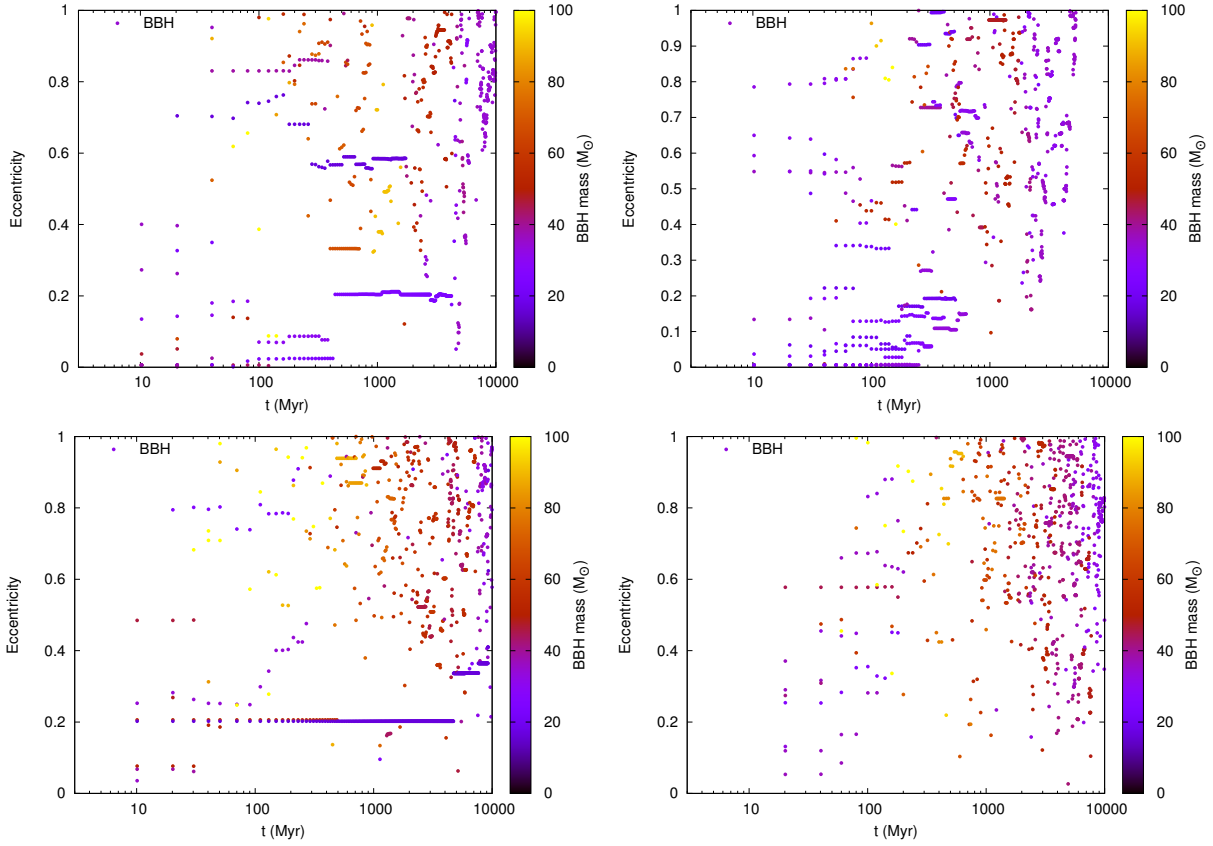


Figure 8. The eccentricities of the BBH population bound to the computed models with $M_{cl}(0) \approx 3.0 \times 10^4 M_{\odot}$, $f_{bin}(0) \approx 0.10$ (top) and $M_{cl}(0) \approx 5.0 \times 10^4 M_{\odot}$, $f_{bin}(0) \approx 0.05$ (bottom) having $Z = 0.001$ (left) and 0.005 (right). See Table 1 and Sec. 2 for these models' details. The colour coding (colour bars) represents the total BBH mass.

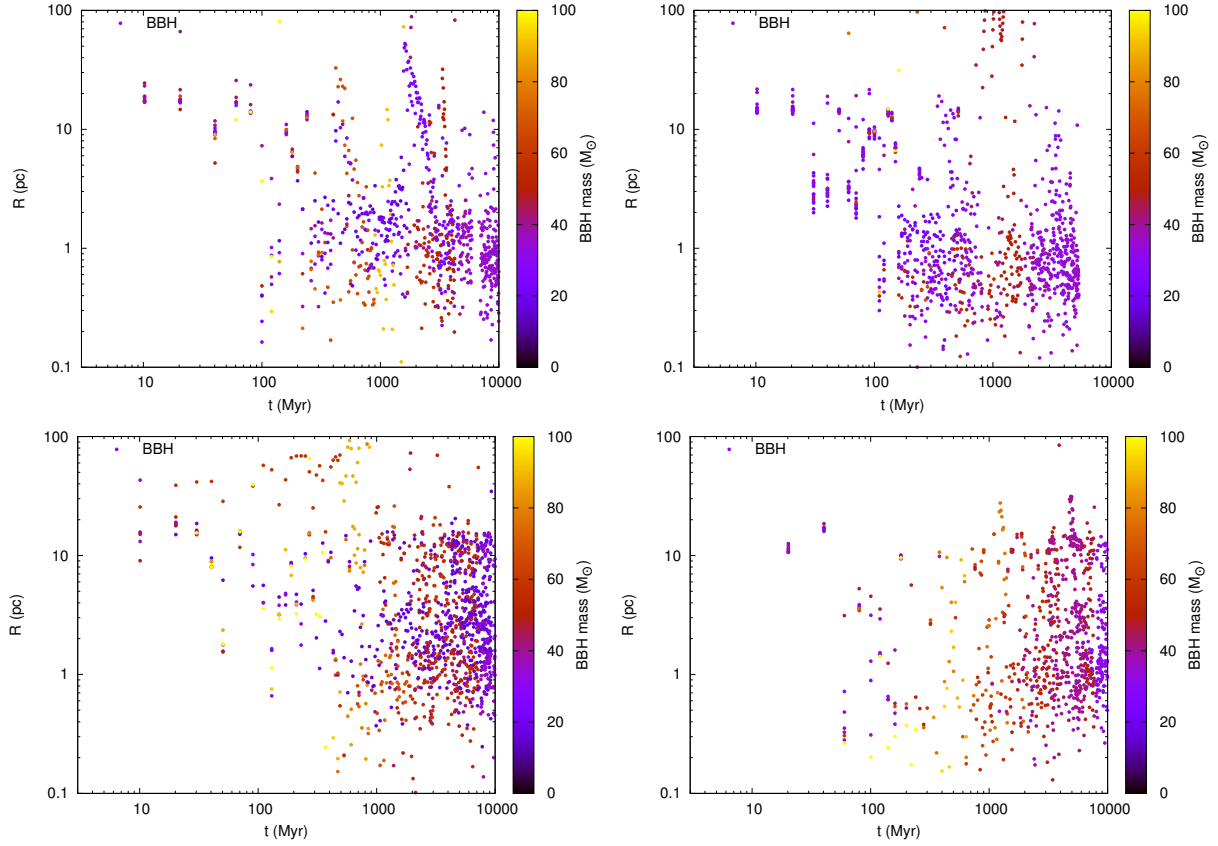


Figure 9. The radial distances w.r.t. the cluster’s density center ($R > 0.1$ pc) of the BBH population bound to the computed models with $M_{cl}(0) \approx 3.0 \times 10^4 M_{\odot}$, $f_{bin}(0) \approx 0.10$ (top) and $M_{cl}(0) \approx 5.0 \times 10^4 M_{\odot}$, $f_{bin}(0) \approx 0.05$ (bottom) having $Z = 0.001$ (left) and 0.005 (right). See Table 1 and Sec. 2 for these models’ details. The colour coding (colour bars) represents the total BBH mass.

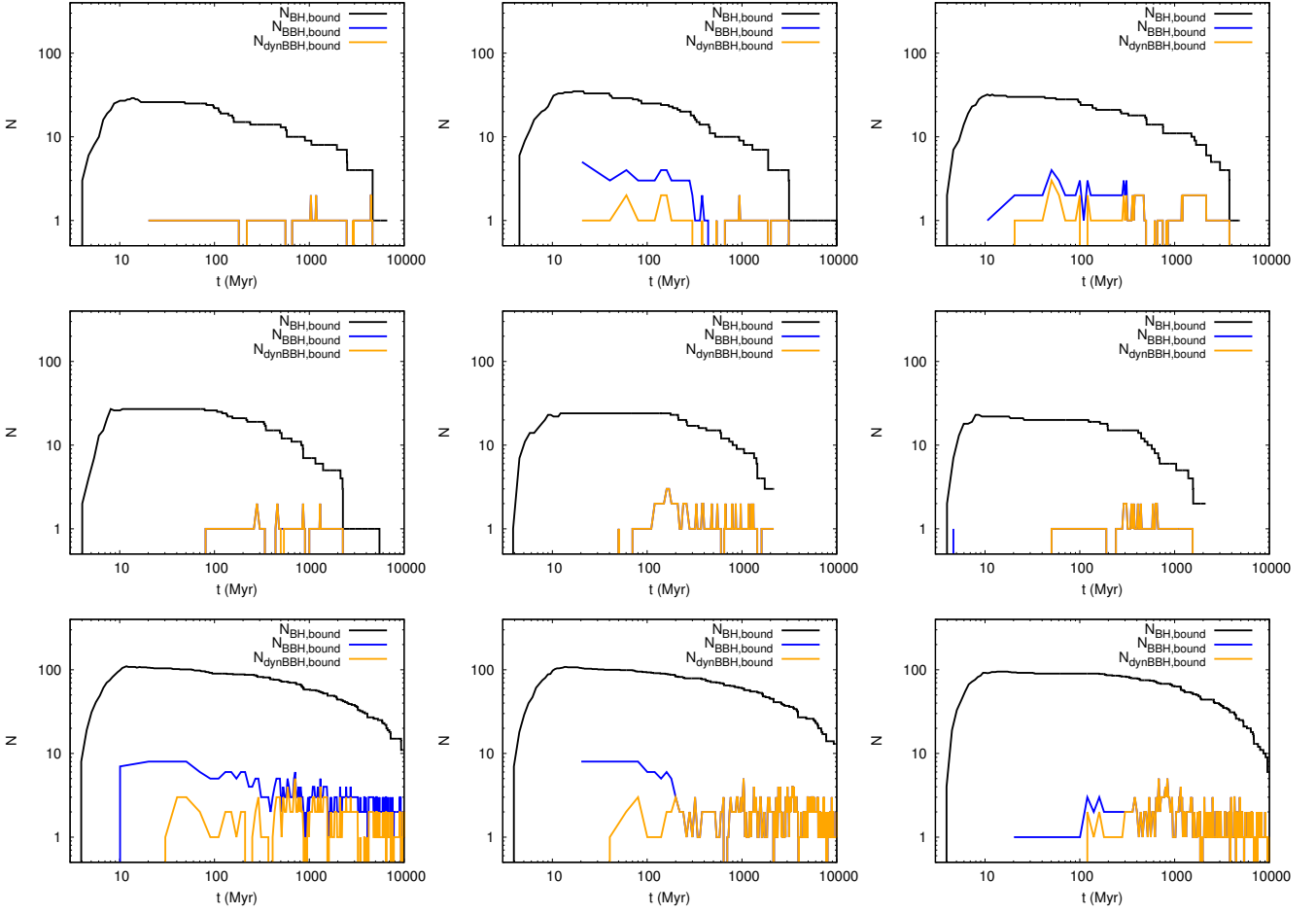


Figure 10. Each of the panels represents the time evolutions of the total number of BHs, $N_{\text{BH,bound}}$ (black line), of the total number of BBHs, $N_{\text{BBH,bound}}$ (blue line), and of the number of dynamically-formed BBHs, $N_{\text{dynBBH,bound}}$ (orange line), that are bound to the cluster. **Top and middle:** for the same models as in Fig. 4 shown in the same order, *i.e.*, those with $M_{cl}(0) \approx 1.5 \times 10^4 M_{\odot}$, $f_{\text{bin}}(0) \approx 0.05, 0.30, 0.50$ (left to right), and $Z = 0.001$ (top), 0.02 (middle). **Bottom:** for the models with $M_{cl}(0) \approx 5.0 \times 10^4 M_{\odot}$, $f_{\text{bin}}(0) \approx 0.05$, $Z = 0.001, 0.005, 0.02$ (left to right).

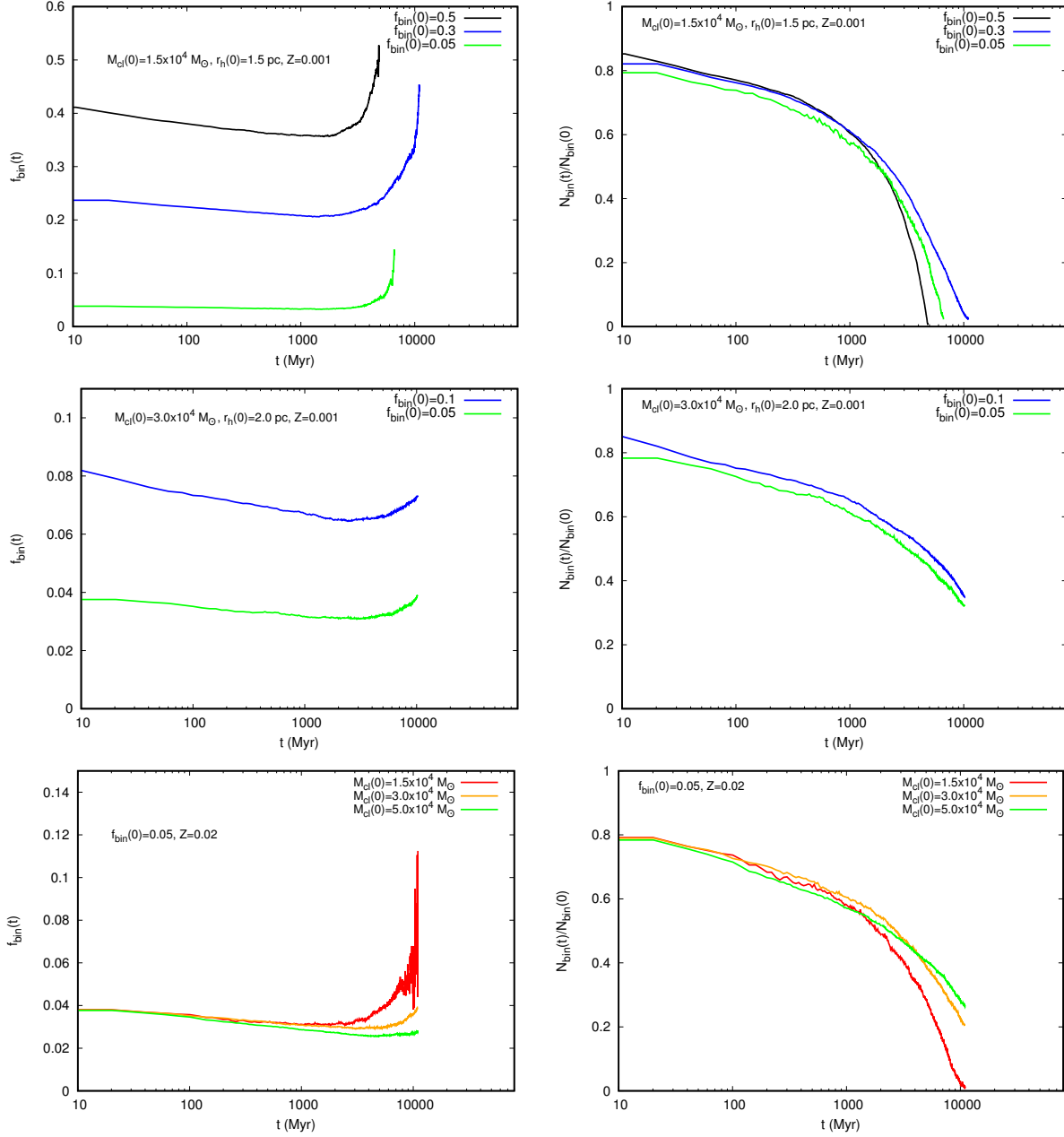


Figure 11. The time evolution of the instantaneous binary fraction, $f_{\text{bin}}(t)$ (left), and the total number of binaries, $N_{\text{bin}}(t)$, normalized w.r.t. the initial number of binaries, $N_{\text{bin}}(0)$ (right), in a representative set of computed models with initial parameters as indicated in the legends (see Table 1).

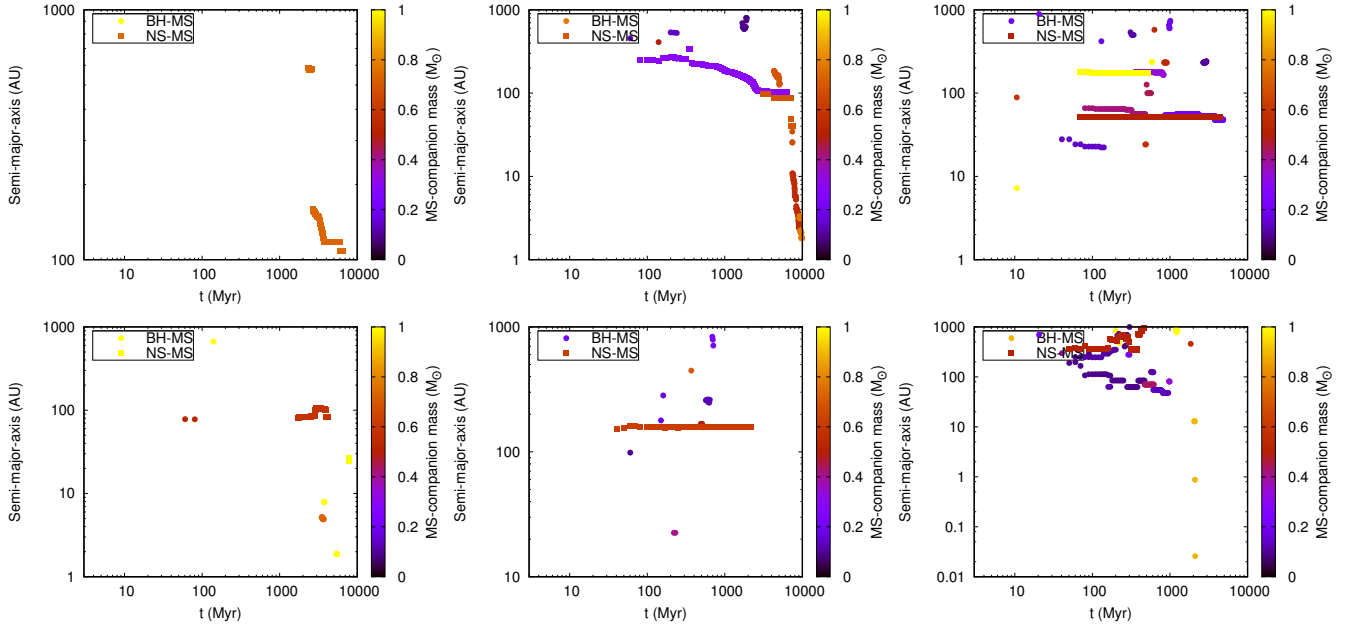


Figure 12. Black hole-main sequence (BH-MS; filled circles) and neutron star-main sequence (NS-MS; filled squares) binaries in the computed $M_{cl}(0) \approx 1.5 \times 10^4 M_{\odot}$ models with evolutionary time, t , as a function of increasing primordial binary fraction, $f_{\text{bin}}(0) \approx 0.05, 0.30, 0.50$ (left to right panels), and for metallicities $Z = 0.001$ (top panel) and 0.02 (bottom panel). On each panel, that represents a particular computed model, the vertical axis is the instantaneous semi-major-axes (< 1000 AU) of the BH-MS/NS-MS binaries that are bound to the cluster snapshot at time t . A continuous trail of points represents a specific BH-MS/NS-MS pair. The colour coding (colour bars) represents the mass of the MS companion. In this and the following Figs. 13, 14, 15, 16, 17, and 18, the “test” runs in Table 1, that include tidal interaction (Sec. 2.2), are excluded, which are presented separately in Fig. 19.

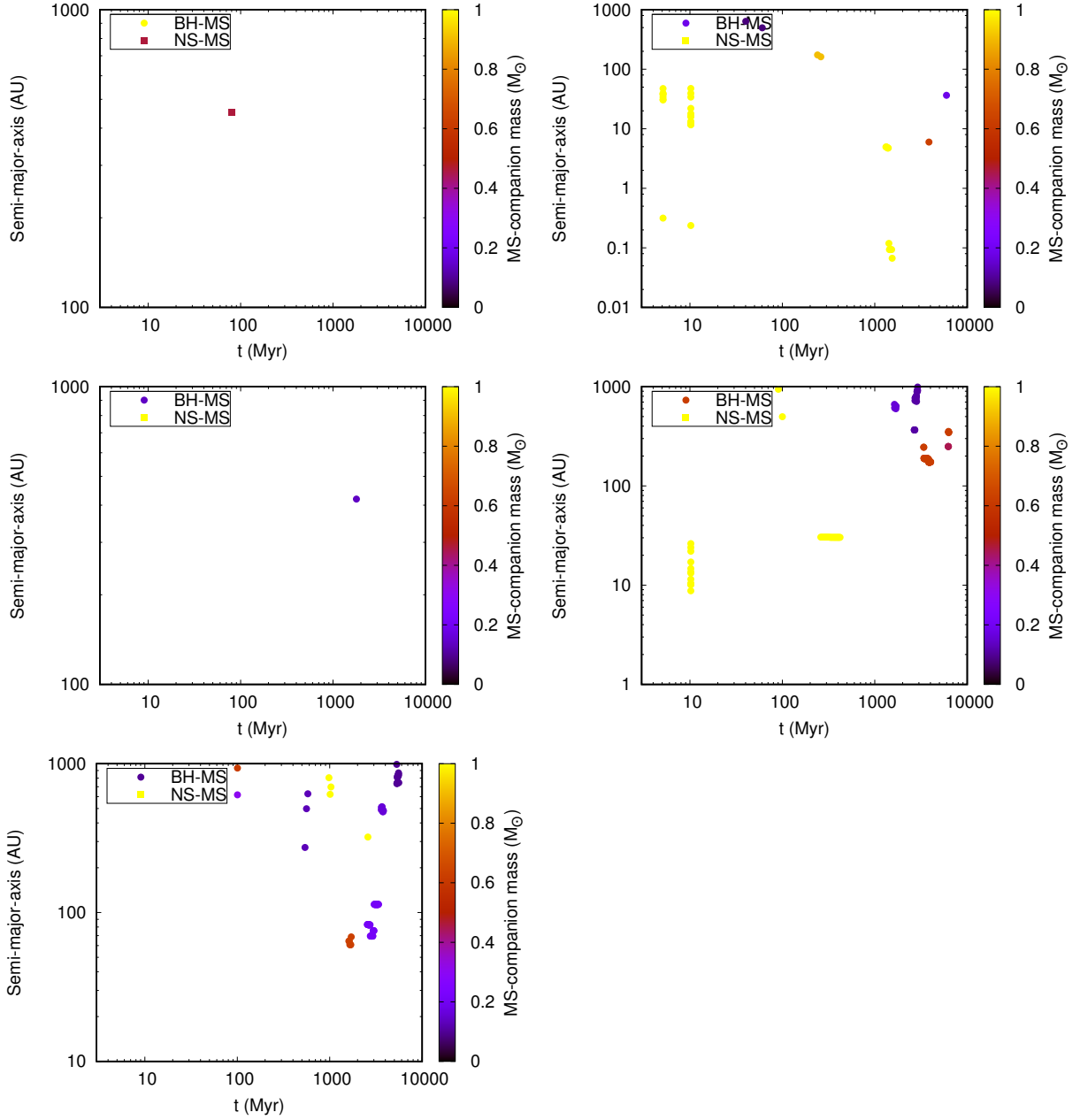


Figure 13. BH-MS/NS-MS binaries in the computed $M_{cl}(0) \approx 3.0 \times 10^4 M_{\odot}$ models with evolutionary time, t , as functions of increasing primordial binary fraction, $f_{\text{bin}}(0) \approx 0.05$ (left), 0.10 (right) and metallicity $Z = 0.001$ (top), 0.005 (middle), and 0.02 (bottom). The legends are the same as in Fig. 12.

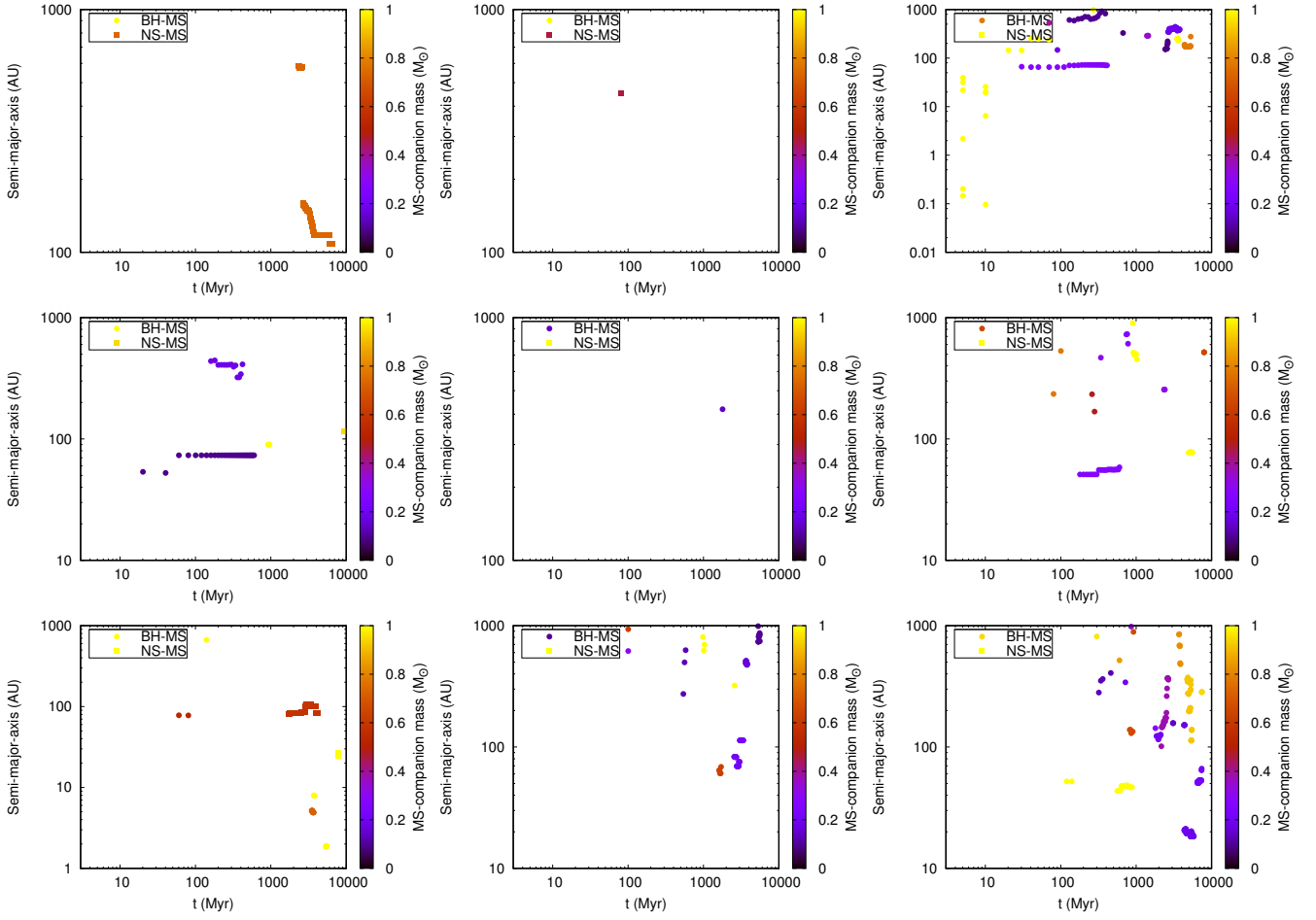


Figure 14. BH-MS/NS-MS binaries in the computed $f_{\text{bin}}(0) \approx 0.05$ models with evolutionary time, t , as a function of increasing $M_{c,i}(0) \approx 1.5 \times 10^4 M_{\odot}$, $3.0 \times 10^4 M_{\odot}$, $5.0 \times 10^4 M_{\odot}$ (left to right) and $Z = 0.001$, 0.005 , 0.02 (top to bottom). The legends are the same as in Fig. 12.

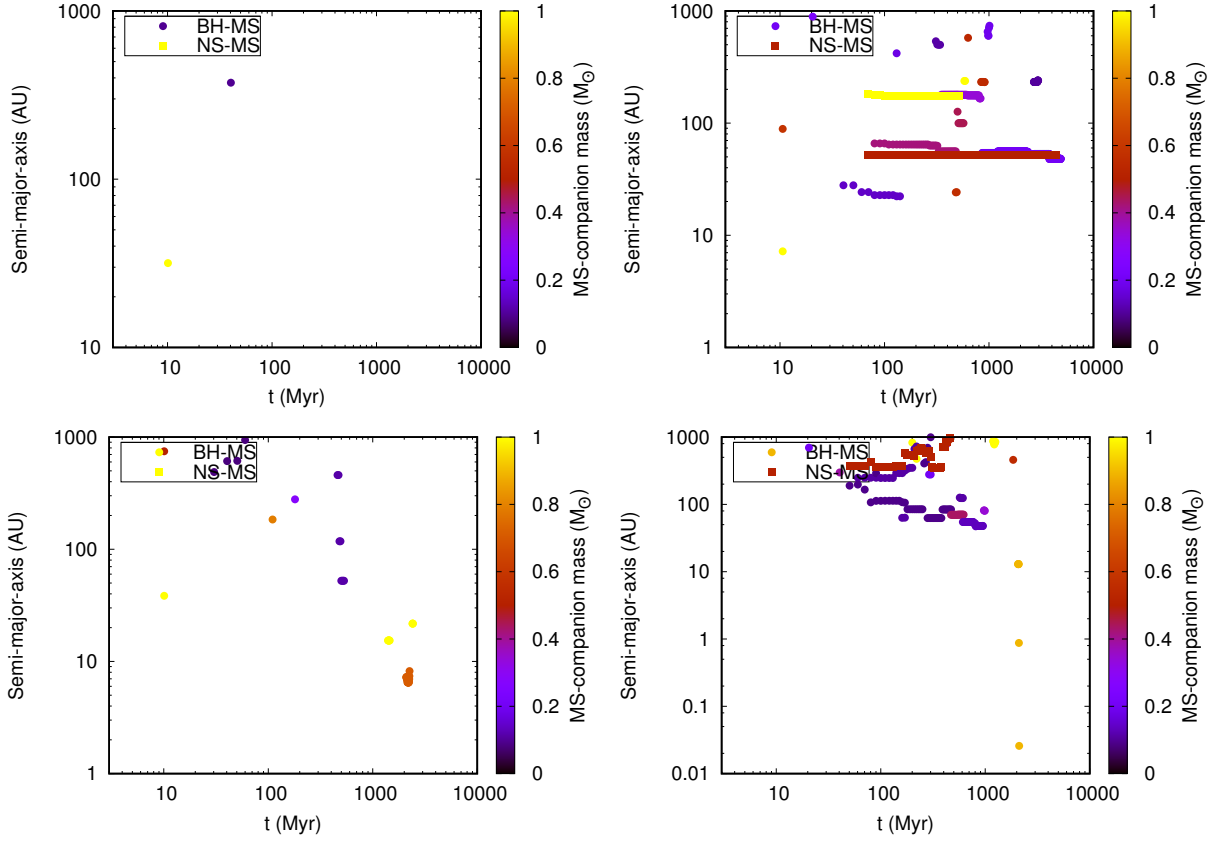


Figure 15. BH-MS/NS-MS binaries in the computed $f_{\text{bin}}(0) \approx 0.50$ models with evolutionary time, t , as a function of increasing $M_{cl}(0) \approx 7.5 \times 10^3 M_{\odot}$ (left) and $1.5 \times 10^4 M_{\odot}$ (right) and for metallicities $Z = 0.001$ (top) and 0.02 (bottom). The legends are the same as in Fig. 12.

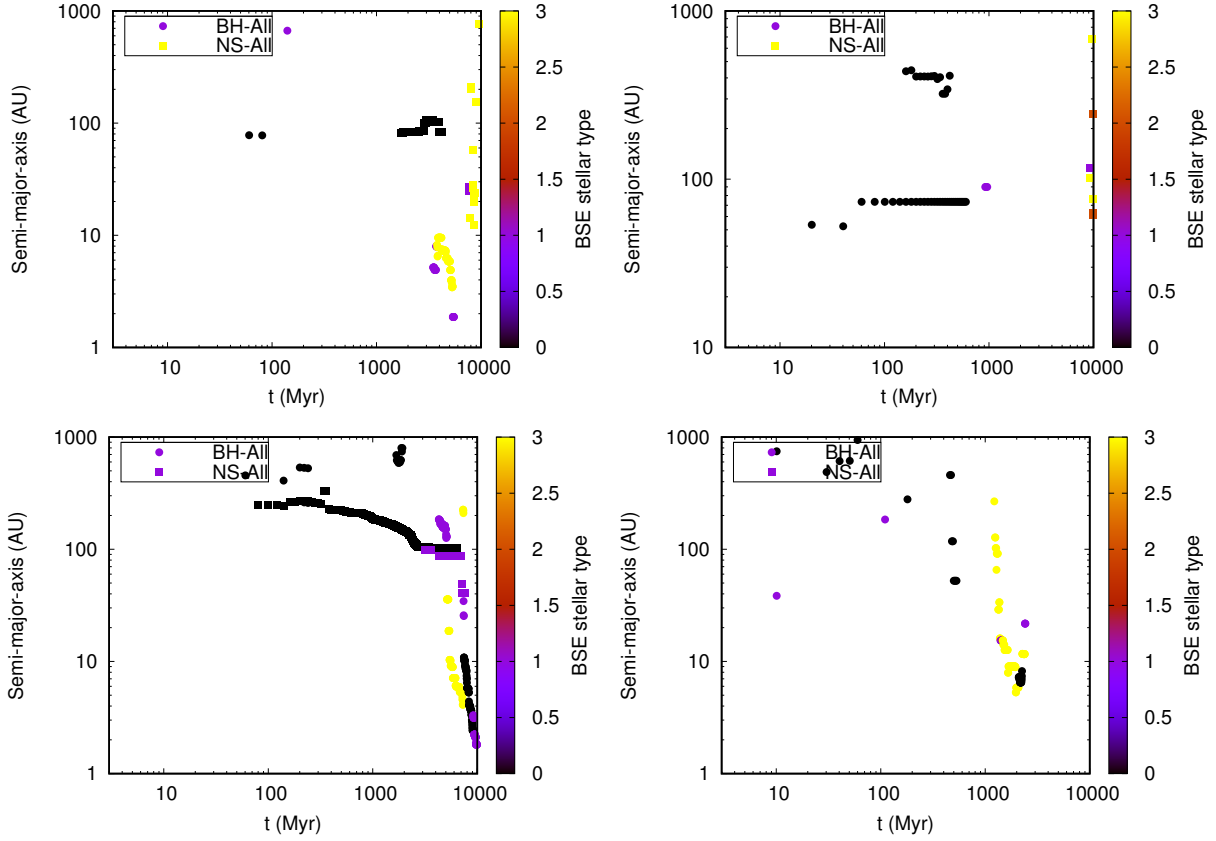


Figure 16. The computed models in Table 1 in which one or more BH/NS (filled circle/square) are found in binaries with a stellar companion that is evolved beyond the MS. In the order top left, top right, bottom left, bottom right with $M_{c,i}(0)$, $f_{\text{bin}}(0)$, Z : $1.5 \times 10^4 M_{\odot}$, 0.05, 0.02; $1.5 \times 10^4 M_{\odot}$, 0.05, 0.005; $1.5 \times 10^4 M_{\odot}$, 0.30, 0.001; $7.5 \times 10^3 M_{\odot}$, 0.50, 0.02. In these panels, the points are colour-coded according to the corresponding stellar companion's BSE stellar type (Hurley et al. 2000), indicating its evolutionary status (0/1 = MS, ≥ 2 = evolved).

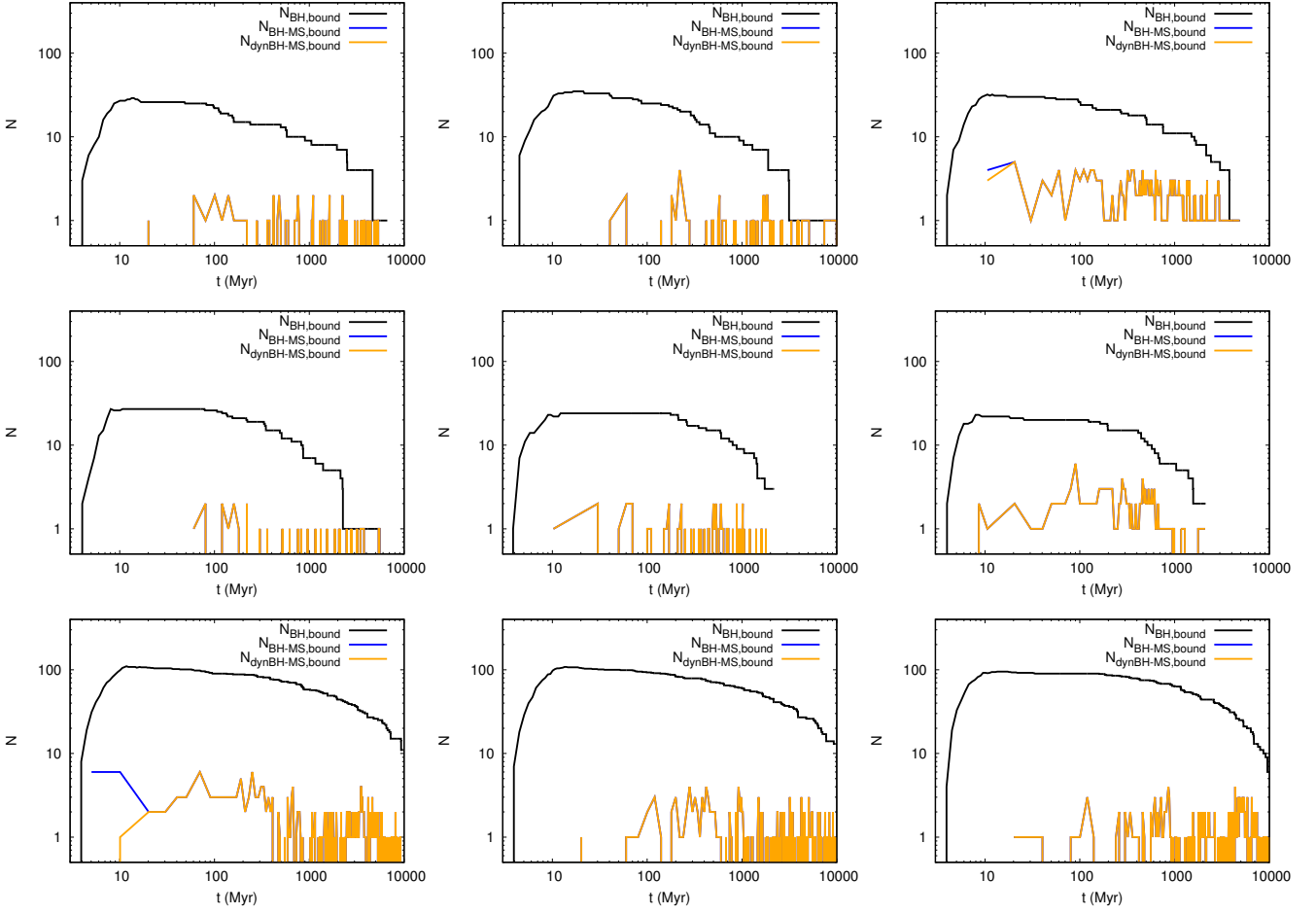


Figure 17. Each of the panels represents the time evolutions of the total number of BHs, $N_{\text{BH,bound}}$ (black line), of the total number of BH-MS binaries, $N_{\text{BH-MS,bound}}$ (blue line), and of the number of dynamically-formed BH-MS binaries, $N_{\text{dynBH-MS,bound}}$ (orange line), that are bound to the cluster. **Top and middle:** for the same models as in Fig. 4 shown in the same order, *i.e.*, those with $M_{\text{cl}}(0) \approx 1.5 \times 10^4 M_{\odot}$, $f_{\text{bin}}(0) \approx 0.05, 0.30, 0.50$ (left to right), and $Z = 0.001$ (top), 0.02 (middle). **Bottom:** for the models with $M_{\text{cl}}(0) \approx 5.0 \times 10^4 M_{\odot}$, $f_{\text{bin}}(0) \approx 0.05$, $Z = 0.001, 0.005, 0.02$ (left to right).

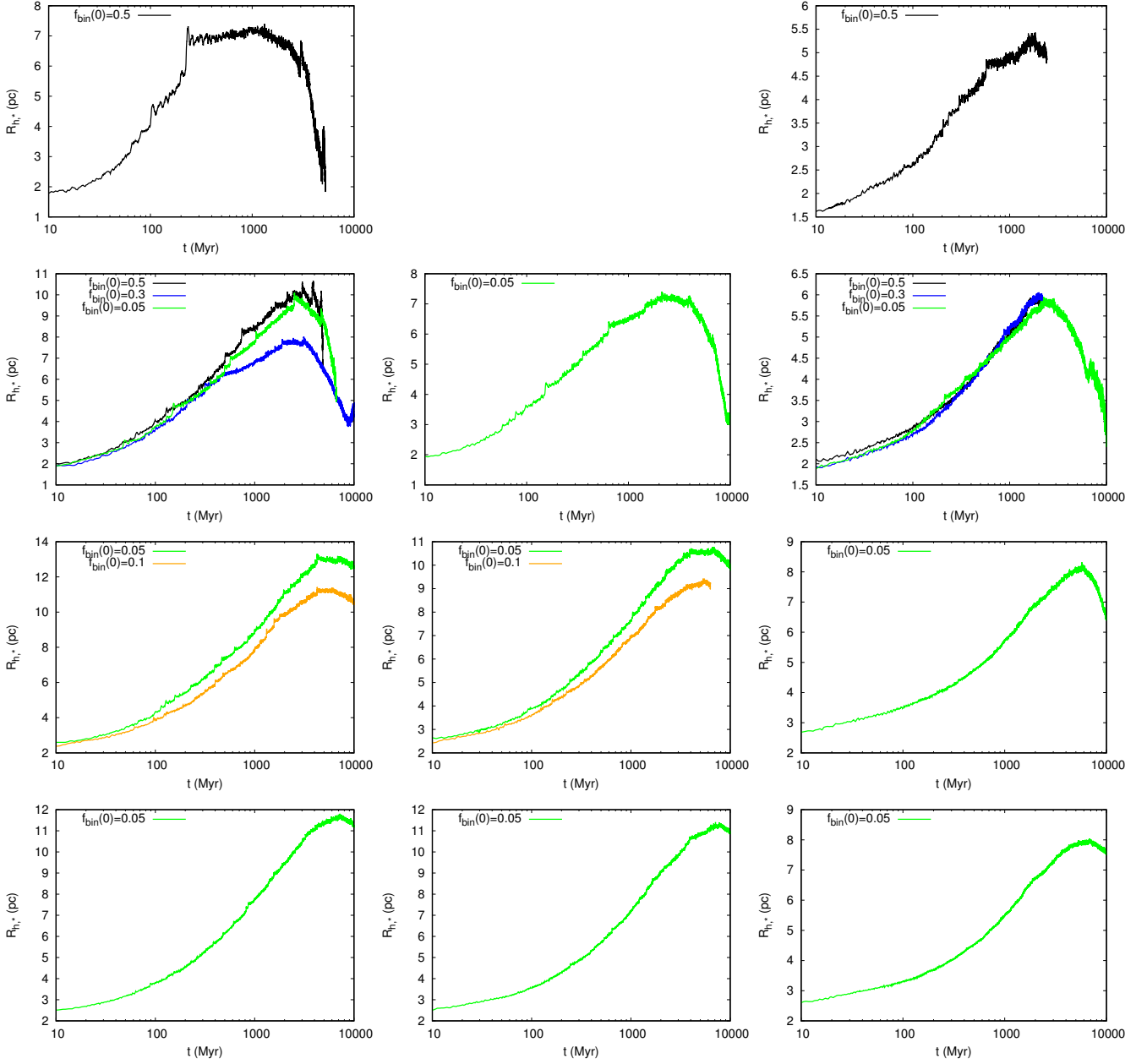


Figure 18. The time evolution of the half-mass radii of the luminous component (all members except the NSs and the BHs), $R_{h,*}$, in the computed models with $M_{cl}(0) \approx 7.5 \times 10^3 M_{\odot}$, $1.5 \times 10^4 M_{\odot}$, $3.0 \times 10^4 M_{\odot}$, and $5.0 \times 10^4 M_{\odot}$ (top to bottom) and $Z = 0.001$, 0.005 , and 0.02 (left to right). The primordial binary fractions are indicated in the legends.

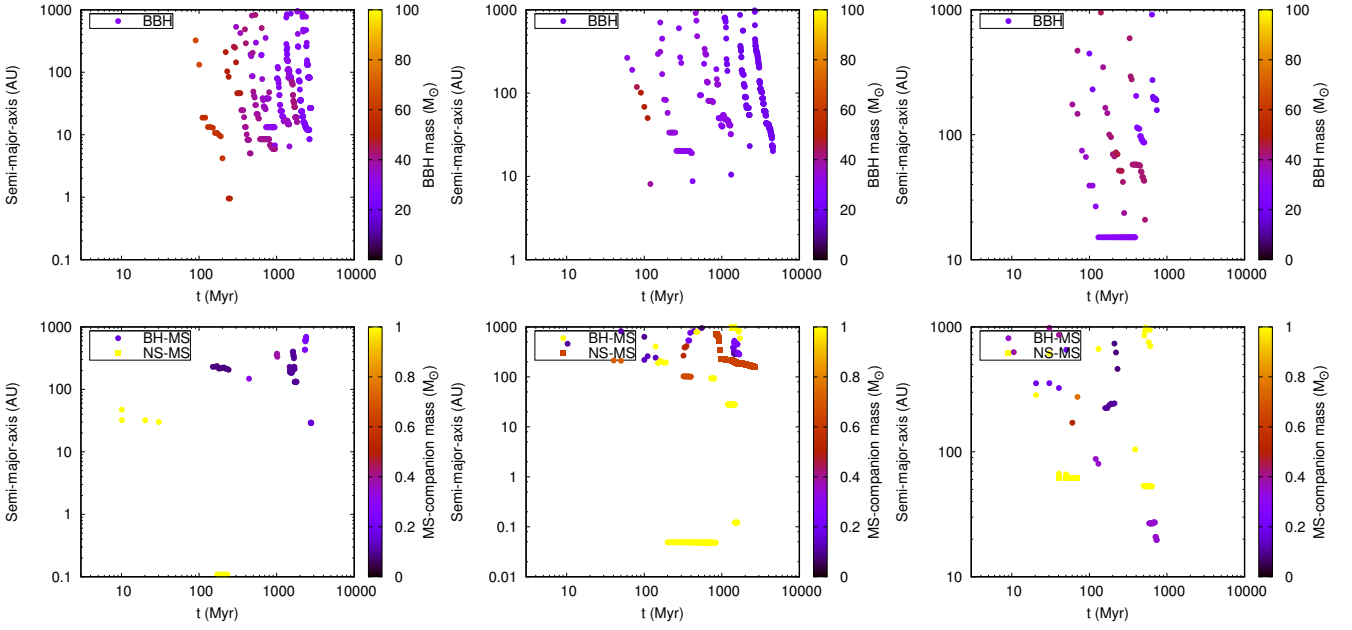


Figure 19. Top: The BBH content in the “test” evolutionary models that include explicit tidal circularization within a binary that contain a non-compact member (see Table 1; Sec. 2.2). The models with $M_{cl}(0) \approx 5.0 \times 10^4 M_{\odot}$; $r_h(0) \approx 2.0$ pc; $f_{bin}(0) \approx 0.05$, $M_{cl}(0) \approx 1.5 \times 10^4 M_{\odot}$; $r_h(0) \approx 1.5$ pc; $f_{bin}(0) \approx 0.30$, and $M_{cl}(0) \approx 1.5 \times 10^4 M_{\odot}$; $r_h(0) \approx 1.5$ pc; $f_{bin}(0) \approx 0.50$ are shown in the panels from left to right respectively. All the three models have $Z = 0.02$. **Bottom:** The BH-MS/NS-MS binaries in these models displayed in the same order.

Table 1: Summary of model evolutionary calculations. The columns from left to right respectively denote: (a) initial mass, $M_{cl}(0)$, of the model cluster, (b) initial half-mass radius, $r_h(0)$, (c) metallicity, Z , (d) overall primordial binary fraction, f_{bin} (see Sec. 2.1), (e) total evolutionary time, T_{evol} , of the model, (f) the number of (triple-mediated) binary black hole (BBH) coalescences, $N_{mrg,in}$, that occurred within the clusters, (g) the number of BBH coalescences (in BBHs that are ejected from the clusters), $N_{mrg,out}$, that occurred outside the clusters within the Hubble time, (h) the number of distinct ‘‘GR slingshots’’ within the clusters, N_{sling} , when available (Sec. 3.2). This table includes the new N-body computations (Sec. 2) and as well those from Banerjee (2018, Paper II) that include a significant population of primordial binaries.

	$M_{cl}(0)/M_{\odot}$	$r_h(0)/pc$	Z/Z_{\odot}	$f_{bin}(0)$	T_{evol}/Gyr	$N_{mrg,in}$	$N_{mrg,out}$	N_{sling}
	7.5×10^3	1.0	0.05	0.50	5.2	1	0	1
	7.5×10^3	1.0	1.00	0.50	2.4	0	0	0
	1.5×10^4	1.5	0.05	0.05	6.6	1	0	1
<i>a</i>	1.5×10^4	1.5	0.05	0.05	9.4	4	0	>10
	1.5×10^4	1.5	0.25	0.05	9.9	1	0	4
	1.5×10^4	1.5	1.00	0.05	11.0	0	0	3
	1.5×10^4	1.5	0.05	0.30	11.0	2	0	1
	1.5×10^4	1.5	1.00	0.30	2.2	0	1	2
	1.5×10^4	1.5	0.05	0.50	4.9	0	0	1
	1.5×10^4	1.5	1.00	0.50	2.1	1	0	1
<i>b</i>	3.0×10^4	2.0	0.05	0.05	10.2	1	0	-
<i>c</i>	3.0×10^4	2.0	0.25	0.05	10.1	4	0	-
	3.0×10^4	2.0	0.25	0.05	10.9	1	0	4
	3.0×10^4	2.0	1.00	0.05	10.9	1	0	0
<i>d</i>	3.0×10^4	2.0	0.05	0.10	10.2	3	0	-
<i>e</i>	3.0×10^4	2.0	0.25	0.10	6.3	3	0	-
	5.0×10^4	2.0	0.05	0.05	11.0	2	1	-
	5.0×10^4	2.0	0.25	0.05	11.0	4	0	-
	5.0×10^4	2.0	1.00	0.05	11.0	2	0	-
<i>f</i>	1.5×10^4	1.5	1.00	0.30	4.6	1	0	0
<i>g</i>	1.5×10^4	1.5	1.00	0.50	0.75	0	0	2
<i>h</i>	5.0×10^4	2.0	1.00	0.05	2.8	2	0	0

a Speed of light $c/100$ assumed for this particular model.

b From Paper II.

c From Paper II.

d From Paper II.

e From Paper II.

f Tidal circularization (NBODY7 option 27 = 1) applied.

g Tidal circularization (NBODY7 option 27 = 1) applied.

h Tidal circularization (NBODY7 option 27 = 1) applied.

References

- Aarseth S. J., 2003, *Gravitational N-Body Simulations*, Cambridge University Press, Cambridge, UK, pp. 430. ISBN 0521432723
- Aarseth S. J., 2012, *MNRAS*, **422**, 841
- Abbott B. P., et al., 2016a, *Physical Review Letters*, **116**, 061102
- Abbott B. P., et al., 2016b, *Physical Review Letters*, **116**, 241103
- Abbott B. P., et al., 2016c, *ApJ*, **818**, L22
- Abbott B. P., et al., 2017a, *Physical Review Letters*, **118**, 221101
- Abbott B. P., et al., 2017b, *Physical Review Letters*, **119**, 141101
- Abbott B. P., et al., 2017c, *ApJ*, **848**, L13
- Abbott B. P., et al., 2017d, *ApJ*, **851**, L35
- Amaro-Seoane P., et al., 2017, ArXiv e-prints (arXiv:1702.00786),
- Antonini F., Rasio F. A., 2016, *ApJ*, **831**, 187
- Antonini F., Chatterjee S., Rodriguez C. L., Morscher M., Pattabiraman B., Kalogera V., Rasio F. A., 2016, *ApJ*, **816**, 65
- Antonini F., Toonen S., Hamers A. S., 2017, *ApJ*, **841**, 77
- Antonini F., Rodriguez C. L., Petrovich C., Fischer C. L., 2018, *MNRAS*, **480**, L58
- Arca-Sedda M., Capuzzo-Dolcetta R., 2017, ArXiv e-prints (arXiv:1709.05567),
- Arca Sedda M., Askar A., Giersz M., 2018, *MNRAS*, **479**, 4652
- Askar A., Szkudlarek M., Gondek-Rosińska D., Giersz M., Bulik T., 2017, *MNRAS*, **464**, L36
- Askar A., Arca Sedda M., Giersz M., 2018, *MNRAS*, **478**, 1844
- Banerjee S., 2017, *MNRAS*, **467**, 524
- Banerjee S., 2018, *MNRAS*, **473**, 909
- Banerjee S., Ghosh P., 2006, *MNRAS*, **373**, 1188
- Banerjee S., Baumgardt H., Kroupa P., 2010, *MNRAS*, **402**, 371
- Belczynski K., Kalogera V., Rasio F. A., Taam R. E., Zezas A., Bulik T., Maccarone T. J., Ivanova N., 2008, *The Astrophysical Journal Supplement Series*, **174**, 223
- Belczynski K., Bulik T., Fryer C. L., Ruitter A., Valsecchi F., Vink J. S., Hurley J. R., 2010, *The Astrophysical Journal*, **714**, 1217
- Belczynski K., Holz D. E., Bulik T., O'Shaughnessy R., 2016, *Nature*, **534**, 512
- Belczynski K., et al., 2017, ArXiv e-prints (arXiv:1706.07053),
- Campanelli M., Lousto C., Zlochower Y., Merritt D., 2007, *ApJ*, **659**, L5
- Chatterjee S., Rodriguez C. L., Rasio F. A., 2017a, *ApJ*, **834**, 68
- Chatterjee S., Rodriguez C. L., Kalogera V., Rasio F. A., 2017b, *ApJ*, **836**, L26
- Chen X., Amaro-Seoane P., 2017, *ApJ*, **842**, L2
- Chomiuk L., Strader J., Maccarone T. J., Miller-Jones J. C. A., Heinke C., Noyola E., Seth A. C., Ransom S., 2013, *ApJ*, **777**, 69
- De Mink S. E., Mandel I., 2016, *MNRAS*, **460**, 3545
- De Mink S. E., Cantiello M., Langer N., Pols O. R., Brott I., Yoon S.-C., 2009, *A&A*, **497**, 243
- Duquennoy A., Mayor M., 1991, *A&A*, **248**, 485
- Farr W. M., Stevenson S., Miller M. C., Mandel I., Farr B., Vecchio A., 2017, *Nature*, **548**, 426
- Fragione G., Pavlík V., Banerjee S., 2018, *MNRAS*, **480**, 4955
- Fryer C. L., 1999, *The Astrophysical Journal*, **522**, 413
- Fryer C. L., Kalogera V., 2001, *The Astrophysical Journal*, **554**, 548
- Geller A. M., Leigh N. W. C., 2015, *ApJ*, **808**, L25
- Geller A. M., de Grijs R., Li C., Hurley J. R., 2015, *ApJ*, **805**, 11
- Gieles M., Larsen S. S., Bastian N., Stein I. T., 2006, *A&A*, **450**, 129
- Giesers B., et al., 2018, *MNRAS*, **475**, L15
- Heggie D. C., 1975, *MNRAS*, **173**, 729
- Heggie D., Hut P., 2003, *The Gravitational Million-Body Problem: A Multidisciplinary Approach to Star Cluster Dynamics*, Cambridge University Press, 372 pp.
- Hoang B.-M., Naoz S., Kocsis B., Rasio F. A., Dosopoulou F., 2018, *ApJ*, **856**, 140
- Hobbs G., et al., 2010, *Classical and Quantum Gravity*, **27**, 084013
- Hughes S. A., 2009, *ARA&A*, **47**, 107
- Hurley J. R., Pols O. R., Tout C. A., 2000, *Monthly Notices of the Royal Astronomical Society*, **315**, 543
- Hurley J. R., Tout C. A., Pols O. R., 2002, *Monthly Notices of the Royal Astronomical Society*, **329**, 897
- Hut P., Bahcall J. N., 1983, *ApJ*, **268**, 319
- Katz B., Dong S., Malhotra R., 2011, *Physical Review Letters*, **107**, 181101
- Khalaj P., Baumgardt H., 2013, *MNRAS*, **434**, 3236
- Kimpson T. O., Spera M., Mapelli M., Ziosi B. M., 2016, *MNRAS*, **463**, 2443
- Kiseleva L. G., Eggleton P. P., Mikkola S., 1998, *MNRAS*, **300**, 292
- Kozai Y., 1962, *The Astronomical Journal*, **67**, 591
- Kremer K., Chatterjee S., Breivik K., Rodriguez C. L., Larson S. L., Rasio F. A., 2018a, *Physical Review Letters*, **120**, 191103
- Kremer K., Chatterjee S., Rodriguez C. L., Rasio F. A., 2018b, *ApJ*, **852**, 29
- Kremer K., Ye C. S., Chatterjee S., Rodriguez C. L., Rasio F. A., 2018c, *ApJ*, **855**, L15
- Kroupa P., 1995, *MNRAS*, **277**, 1491
- Kroupa P., 2001, *MNRAS*, **322**, 231
- Kulkarni S. R., Hut P., McMillan S., 1993, *Nature*, **364**, 421
- Larsen S. S., 2009, *Astronomy and Astrophysics*, **494**, 539
- Leigh N. W. C., Geller A. M., 2013, *MNRAS*, **432**, 2474
- Leigh N., Sills A., 2011, *MNRAS*, **410**, 2370
- Leigh N. W. C., Lützgendorf N., Geller A. M., Maccarone T. J., Heinke C., Sesana A., 2014, *MNRAS*, **444**, 29
- Leigh N. W. C., Giersz M., Marks M., Webb J. J., Hypki A., Heinke C. O., Kroupa P., Sills A., 2015, *MNRAS*, **446**, 226
- Lithwick Y., Naoz S., 2011, *ApJ*, **742**, 94
- Liu B., Lai D., 2017, *ApJ*, **846**, L11
- Lützgendorf N., et al., 2016, in Meiron Y., Li S., Liu F.-K., Spurzem R., eds, *IAU Symposium Vol. 312, Star Clusters and Black Holes in Galaxies across Cosmic Time*. pp 181–188 (arXiv:1501.07441), doi:10.1017/S1743921315007784
- Mandel I., Farmer A., 2017, *Nature*, **547**, 284
- Mapelli M., 2016, *MNRAS*, **459**, 3432
- Mapelli M., 2018, in *Journal of Physics Conference Series*. p. 012001, doi:10.1088/1742-6596/957/1/012001
- Mapelli M., Ripamonti E., Zampieri L., Colpi M., 2011, *MNRAS*, **416**, 1756
- Mapelli M., Zampieri L., Ripamonti E., Bressan A., 2013, *MNRAS*, **429**, 2298
- Mapelli M., Giacobbo N., Ripamonti E., Spera M., 2017, *MNRAS*, **472**, 2422
- Marchant P., Langer N., Podsiadlowski P., Tauris T. M., Moriya T. J., 2016, *A&A*, **588**, A50
- Mardling R. A., Aarseth S. J., 2001, *MNRAS*, **321**, 398
- Mikkola S., Aarseth S. J., 1993, *Celestial Mechanics & Dynamical Astronomy*, **57**, 439
- Mikkola S., Aarseth S., 2002, *Celestial Mechanics and Dynamical Astronomy*, **84**, 343
- Mikkola S., Merritt D., 2008, *The Astronomical Journal*, **135**, 2398
- Mikkola S., Tanikawa K., 1999, *Monthly Notices of the Royal Astronomical Society*, **310**, 745
- Miller-Jones J. C. A., et al., 2015, *MNRAS*, **453**, 3918
- Milliman K. E., Mathieu R. D., Geller A. M., Gosnell N. M., Meibom S., Platais I., 2014, *AJ*, **148**, 38
- Morscher M., Umbreit S., Farr W. M., Rasio F. A., 2013, *ApJ*, **763**, L15
- Morscher M., Pattabiraman B., Rodriguez C., Rasio F. A., Umbreit S., 2015, *The Astrophysical Journal*, **800**, 9
- Nishizawa A., Sesana A., Berti E., Klein A., 2017, *MNRAS*, **465**, 4375

- Nitadori K., Aarseth S. J., 2012, *Monthly Notices of the Royal Astronomical Society*, 424, 545
- Park D., Kim C., Lee H. M., Bae Y.-B., Belczynski K., 2017, *MNRAS*, 469, 4665
- Peters P. C., 1964, *Physical Review*, 136, 1224
- Plummer H. C., 1911, *MNRAS*, 71, 460
- Podsiadlowski P., Langer N., Poelarends A. J. T., Rappaport S., Heger A., Pfahl E., 2004, *The Astrophysical Journal*, 612, 1044
- Rodriguez C. L., Chatterjee S., Rasio F. A., 2016, *Physical Review D*, 93
- Rodriguez C. L., Amaro-Seoane P., Chatterjee S., Rasio F. A., 2018, *Phys. Rev. Lett.*, 120, 151101
- Samsing J., 2018, *Phys. Rev. D*, 97, 103014
- Samsing J., D’Orazio D. J., 2018, *MNRAS*(arXiv:1804.06519),
- Samsing J., Ramirez-Ruiz E., 2017, *ApJ*, 840, L14
- Samsing J., MacLeod M., Ramirez-Ruiz E., 2014, *ApJ*, 784, 71
- Sana H., Evans C. J., 2011, in Neiner C., Wade G., Meynet G., Peters G., eds, IAU Symposium Vol. 272, Active OB Stars: Structure, Evolution, Mass Loss, and Critical Limits. pp 474–485 (arXiv:1009.4197), doi:10.1017/S1743921311011124
- Sana H., et al., 2013, *A&A*, 550, A107
- Sesana A., 2016, *Physical Review Letters*, 116, 231102
- Shishkovsky L., et al., 2018, *ApJ*, 855, 55
- Sigurdsson S., Hernquist L., 1993, *Nature*, 364, 423
- Sigurdsson S., Phinney E. S., 1993, *ApJ*, 415, 631
- Silsbee K., Tremaine S., 2017, *ApJ*, 836, 39
- Sippel A. C., Hurley J. R., 2013, *MNRAS*, 430, L30
- Spitzer L., 1987, Dynamical evolution of globular clusters, Princeton University Press, Princeton, NJ, 191 p.
- Stevenson S., Vigna-Gómez A., Mandel I., Barrett J. W., Neijssel C. J., Perkins D., de Mink S. E., 2017, *Nature Communications*, 8, 14906
- Strader J., Chomiuk L., Maccarone T. J., Miller-Jones J. C. A., Seth A. C., 2012, *Nature*, 490, 71
- Vink J. S., de Koter A., Lamers H. J. G. L. M., 2001, *Astronomy and Astrophysics*, 369, 574
- Wang L., et al., 2016, *Mon. Not. R. Astron. Soc.*, 458, 1450
- Wen L., 2003, *ApJ*, 598, 419
- Ziosi B. M., Mapelli M., Branchesi M., Tormen G., 2014, *MNRAS*, 441, 3703